

# Electron properties of carbon nanotubes in a periodic potential

Dmitry S. Novikov\*

Department of Electrical Engineering and Department of Physics, Princeton University, Princeton, NJ 08544 and  
Department of Physics, Massachusetts Institute of Technology, Cambridge, MA 02139

(Dated: February 8, 2020)

Coupling of nanotube electrons to an external periodic potential is suggested as a means to study effects of strong electron interactions, including pinning of the Wigner crystal, and Bragg diffraction in a Luttinger liquid of multiple flavors. Electron interactions result in a devil's staircase of incompressible states that correspond to the electron density (counted from half-filling) commensurate with the potential. Excitation gaps are estimated by generalizing the theory of commensurate-incommensurate transitions for the case of interacting Dirac fermions of multiple polarizations. In the limit when electron wave functions are extended, incompressible electron states and excitation gaps are described in terms of the narrow gap four-flavor Luttinger liquid. Charge gaps are enhanced due to quantum fluctuations of the neutral sector, whereas neutral excitations are governed by the effective  $SU(4) \simeq O(6)$  Gross-Neveu Lagrangian. In the opposite limit of the tightly bound electrons, effects of exchange are unimportant, and the system behaves as a single fermion mode that represents a Wigner crystal locked by the external potential. The phase diagram is drawn using the effective spinless Dirac Hamiltonian derived in this limit. Incompressible states can be detected in the adiabatic transport setup proposed in [V.I. Talyanskii, D.S. Novikov, B.D. Simons, L.S. Levitov, Phys. Rev. Lett. **87**, 276802 (2001)], in which a slowly moving potential can induce a quantized current, with a possibility to pump a fraction of an electron charge per cycle.

PACS numbers: 71.10.Pm, 85.35.Kt, 64.70.Rh

## I. INTRODUCTION

Since their discovery<sup>1</sup>, carbon nanotubes (NTs) remain in focus of both basic and applied research.<sup>2,3</sup> Besides their important technological potential,<sup>4-8</sup> nanotubes are a testing ground for novel physical phenomena involving strong electron interactions. Theoretically, they are considered perfect systems to study Tomonaga-Luttinger liquid effects.<sup>9-14</sup> Experimentally, effects of electron-electron interactions in nanotubes have been observed in the Coulomb blockade peaks in transport,<sup>15,16</sup> in the power law temperature and bias dependence of the tunneling conductance,<sup>17-19</sup> and in the power law dependence of the angle-integrated photoemission spectra.<sup>20</sup>

In the present work we suggest coupling of an external periodic potential to the nanotube electronic system as a probe of both Tomonaga-Luttinger effects, and of the 1d Wigner crystallization, by employing commensurability. We focus on the electron properties of single-walled carbon nanotubes in a periodic potential whose period  $\lambda_{\text{ext}}$  is much greater than the NT radius  $a$ ,  $\lambda_{\text{ext}} \gg a$ . Such a potential can be realized using optical methods, by gating, or by an acoustic field. In all of these cases, realistic period  $\lambda_{\text{ext}}$  is of the order 0.1–1  $\mu\text{m}$ . As shown below, effects of the Tomonaga-Luttinger correlations on the Bragg diffraction of electrons, realization of the  $SU(4)$  invariant spin excitations, as well as pinning of the Wigner crystal can be demonstrated in such a setup depending on the applied potential and on the NT parameters. Our main finding is the devil's staircase of *incompressible electron states* whose existence relies on electron-electron interactions.<sup>21</sup>

A nanotube is a unique system to study effects of strong electron interactions. Indeed, low dimensional-

ity increases interaction effects; the Dirac nature<sup>2</sup> of the single particle spectrum allows for essentially *exact* bosonized treatment of electron-electron interactions even at low density (near the bottom of the band) via the massive Thirring – quantum sine-Gordon duality;<sup>22,23</sup> spin and Brillouin zone degeneracy<sup>2</sup> result in the presence of the *four* types of Dirac fermions with approximate  $SU(4)$  symmetry of the problem that allows one to realize spin excitations of high symmetry;<sup>13</sup> robust chemical and mechanical NT properties result in very low disorder; finally, diverse methods of nanotube synthesis, a variety of available nanotube chiralities and of the ways of coupling to the nanotube electron system allow one to explore a wide region of the phase diagram.

Below we will identify incompressible electron states (characterized by excitation gaps) that arise when the average NT electron number density  $\bar{\rho}$  counted from half-filling is *commensurate* with the potential period:

$$\bar{\rho} = \frac{m_{\text{tot}}}{\lambda_{\text{ext}}}, \quad m_{\text{tot}} = 4m. \quad (1)$$

In Eq. (1)  $m$  is the number of fermions of each of the four types (called below “flavors”) per potential period  $\lambda_{\text{ext}}$ .

At what values of the density  $m$  the spectral gaps can open? In the absence of interactions, the theory of the Bloch electron results in the spectrum of *minibands* separated by *minigaps* as a consequence of the Bragg diffraction on the external periodic potential. Filling an integer number  $m$  of minibands corresponds to adding  $m$  electrons per “unit cell” (potential period). This results in the condition (1) with *integer* density<sup>24</sup>  $m = 0, \pm 1, \pm 2, \dots$ , which can be thought of as the commensurability requirement due to the wave nature of electrons.

In the present work we will show that electron–electron interactions dramatically change the spectrum, adding incompressible states at the *rational* densities  $m = p/q$ . This interaction–induced commensurability can be qualitatively understood as a result of pinning of the Wigner crystal by the external potential, linking this problem to that of the commensurate–incommensurate transitions. In such a fractional– $m$  state, the NT electron system is “locked” by the external potential into a  $q\lambda_{\text{ext}}$ –periodic structure schematically represented in Fig. 1. Naturally, the states with the lower denominator  $q$  will be more pronounced. Realistically, due to the finite system size and finite temperature, only a few states with small enough  $q$  could be reliably detected. However, these fractional– $m$  states are important as the corresponding minigaps are interaction–induced (and vanish in the noninteracting limit). Therefore, if measured, such minigaps would provide a direct probe of the strength of interactions between the NT electrons.

To detect incompressible electron states, including the ones with fractional  $m$ , one can utilize the recent proposal<sup>24</sup> of the adiabatic pump in a nanotube. Ref. 24 suggests taking advantage of the semi–metallic nature of the nanotube dispersion to realize the Thouless pump.<sup>28</sup> In such a setup, a *quantized current* is predicted to arise whenever the chemical potential is inside the minigap created by the adiabatically slowly moving external periodic potential. In the presence of electron interactions, commensurability (1) will result in the adiabatic current corresponding to pumping of the *fractional charge per cycle*. In other words, electron interactions could allow one to realize adiabatic pumping of charge at the *fraction* of the base frequency of the potential modulation.

In connection with the adiabatic current quantization, we note a parallel between our system and the quantum Hall effect. In both cases, commensurability with an external electromagnetic field yields incompressible states, spectral gaps, and the non–dissipative current quantization. Moreover, it is the electron interactions that yield additional incompressible states at the fractional filling factors and result in the corresponding non–dissipative transport. A related QHE analogy that exploits commensurability has been proposed recently by Kane *et al.*<sup>25</sup>

This paper is organized as follows.

In the next Section we discuss the nature of incompressible states qualitatively. In Section III we introduce the model Hamiltonian. In Section IV as a warm–up we consider the noninteracting problem. In Section V we bosonize the many–body Hamiltonian.

Section VI is central. There, we generalize the phase soliton method for the nanotube electrons in the periodic potential utilizing the bosonized description. We also show that an external periodic potential naturally distinguishes between qualitatively different regimes: Bragg diffraction in a narrow–gap Luttinger liquid (corresponding to the electron wavefunctions extended over a few periods of the potential), and pinning of the Wigner crystal (corresponding to electrons localized in the potential

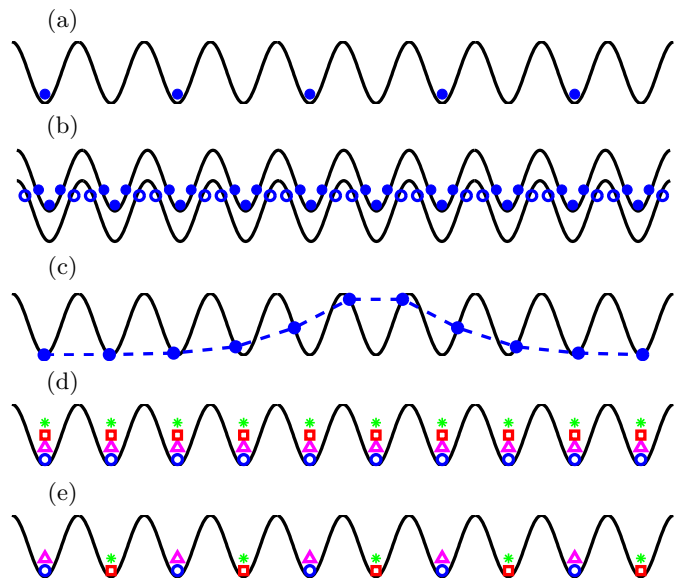


FIG. 1: Incompressible electron states (schematic). (a) The  $(1/2, 0)$  state with  $m_{\text{tot}} = 1/2$ . (b) The  $(3, 2)$  state with  $m_{\text{tot}} = 1$ . Large potential amplitude breaks the Dirac “vacuum” placing holes (open circles) into the potential maxima. (c) An example of the *phase soliton excitation* over the  $(1, 0)$  state. Excitation gap is given by the phase soliton energy. (d) The  $m = 1$  incompressible state that is allowed by the Bloch theory of non–interacting nanotube electrons. Four kinds of labels mark centers of the solitons of the bose fields that correspond to the NT fermions of the four flavors. (e) The simplest interaction–induced  $m = 1/2$  state. Fermions of the same flavor avoid each other due to the Pauli principle.

minima). The choice between the two regimes is determined by the saddle point of the total action for the four bosonic modes. We also discuss the role of quantum fluctuations.

In Section VII we consider the Bragg diffraction limit, whereas in Section VIII we focus on the pinned Wigner crystal. In Section IX we outline and discuss the phase diagram in the semiclassical (Wigner crystal) limit.

In Section X we discuss the experimental ways to observe incompressible states, and conclude in Section XI.

## II. QUALITATIVE PICTURE

### A. Semiclassical picture of interaction–induced incompressible states

Existence of interaction–induced incompressible electron states can be linked to the well–studied problem of classical commensurate–incommensurate transitions [see *e.g.* the review<sup>29</sup>]. Indeed, we show that in the semiclassical limit, when the electron wavefunctions are strongly localized within each potential period  $\lambda_{\text{ext}}$ , the spectrum is the devil’s staircase. Incompressible states in this limit represent locking of the Wigner crystal of electrons by the

periodic potential at commensurate densities. Gaps open at rational densities  $m_{\text{tot}}$ , and Coulomb interaction sets the gap energy scale. An example of such a state with  $m_{\text{tot}} = 1/2$  is shown schematically in Fig. 1(a).

Even within the semiclassical picture, the nanotube electron system exhibits unique features. The Dirac character of nanotube electrons brings about a set of incompressible states in which the Dirac “vacuum” is broken when the potential amplitude exceeds the gap at half-filling. In this case, *different* incompressible states can arise at the *same* total density  $m_{\text{tot}} = n_e - n_h$ . To characterize these states we specify the pair of numbers  $(n_e, n_h)$  of *electrons* and *holes* in the potential minima and maxima correspondingly. An example of the (3, 2) state with  $m_{\text{tot}} = 1$  is schematically shown in Fig. 1(b). In the classical limit, each commensurate state [with rational  $(n_e, n_h)$ ] is incompressible (i.e. characterized by a finite excitation gap) since it costs a finite energy to add one more particle to the system. This energy can be estimated as that of a *phase soliton* that describes the distortion of the regular periodic charge configuration, as illustrated for the (1, 0) state in Fig. 1(c).

Representing an excitation in a commensurate phase by a phase soliton was utilized in the past in various contexts. The model of locking a system into a commensurate state was first suggested in the work of Frenkel and Kontorova.<sup>30</sup> Later, it was re-discovered and solved by Frank and van der Merwe<sup>31</sup> in the context of atoms ordering on crystal surfaces, and by Dzyaloshinskii<sup>32</sup> describing a transition to the state with a helical magnetic structure. The general theory of commensurate-incommensurate phase transitions has been finalized by Pokrovsky and Talapov.<sup>33</sup>

## B. Bragg diffraction vs. pinned Wigner crystal

A novel important feature of the problem with the nanotube electrons is the presence of the *four* types (“flavors”) of the Dirac fermions.<sup>2</sup> The low energy interacting theory possesses the SU(4) symmetry with respect to the rotations in the space of the fermion flavors. The flavor physics requires developing the many-body quantum-mechanical generalization of the phase soliton theory<sup>33</sup> for the case of multiple polarizations even in the limit of the strong Coulomb repulsion.

Quantum-mechanical treatment of interacting nanotube electrons is natural in the bosonized framework, by utilizing the massive Thirring — quantum sine-Gordon duality.<sup>22,23</sup> In this picture, a Dirac fermion corresponds to the sine-Gordon soliton whose size scales inversely with the Dirac gap. We underscore the importance of the Dirac character of the NT electrons by stressing that the conventional bosonization implies a linearized dispersion near the Fermi points and, as a result, it describes the hydrodynamic density modes extended over the length of the system. To study the effects of commensurability or crystallization one needs to include the curvature of

the dispersion, that could generate a finite *length scale* for an excitation. Fortunately, in contrast to a generic electron dispersion, *massive* Dirac fermions can still be bosonized, with the curvature of the dispersion controlled by the Dirac gap.

The presence of the four flavors of the massive Dirac fermions results in the bosonized nonlinear theory  $\mathcal{L}[\theta^0, \theta^a]$  of the four interacting sine-Gordon modes. The SU(4) symmetry of the nanotube electrons brings an important simplification yielding only *two* different kinds of modes<sup>13,24</sup>: the charge mode  $\theta^0$  and the three neutral flavor modes  $\theta^a$ ,  $a = 1, 2, 3$ . When the Coulomb repulsion is strong, the charge mode is stiff, whereas the flavor modes remain soft, their quantum fluctuations renormalizing couplings. As a consequence, only *two* soliton length scales emerge, the charge,  $l_{\text{ch}}$ , and the flavor,  $l_{\text{fl}}$ , with  $l_{\text{ch}} \gg l_{\text{fl}}$  in the limit of the strong repulsion.

In the absence of external potential, an electron corresponds to the *composite soliton* of the action  $\mathcal{L}[\theta^0, \theta^a]$  in which the charge field  $\theta^0$  varies on the scale  $l_{\text{ch}}$  and the neutral fields  $\theta^a$  vary on the scale  $l_{\text{fl}}$  providing a particular flavor to the electron.<sup>13</sup> In this picture, the classical coordinate of an electron corresponds to the center of the composite soliton. Effects of exchange correspond to overlap of the flavor soliton cores of the composite solitons, whereas the Coulomb interaction is represented by the overlap of the charge solitons. At finite electron density the ground state is a compressible lattice of such composite objects.

When effects of exchange are small, the lattice of composite solitons describes the semi-classical one-dimensional Wigner crystal. This happens when the interparticle separation is greater than the flavor soliton size,  $\rho^{-1} \gg l_{\text{fl}}$ . Since there is no phase transition in one dimension, the crossover between the limits of the Luttinger liquid of delocalized electrons ( $\rho^{-1} \ll l_{\text{fl}}$ ) and of the semi-classical Wigner crystal ( $\rho^{-1} \gg l_{\text{fl}}$ ) happens smoothly, although physically these limits are very different. One or the other limit is selected by the *saddle point* of the bosonized action for the four modes.

External periodic potential *locks* the system into an incompressible state when the electron density (1) is commensurate with the potential period. An incompressible state corresponds to the train of the composite solitons of different flavors, commensurate with the external potential. Such a state is characterized by an average number  $m$  of the composite solitons of each flavor per potential period  $\lambda_{\text{ext}}$ , in accord with Eq. (1). In Fig. 1(d,e) centers of solitons that represent electrons of different flavors are marked by different symbols. In accord with the above, such a locking is only possible when the curvature of the Dirac electron dispersion (NT gap at half-filling) is nonzero, since the curvature gives rise to the finite soliton sizes  $l_{\text{ch}}$  and  $l_{\text{fl}}$ . For the strictly linear dispersion (as in the armchair nanotube) both of these scales are infinite, and the minigaps do *not* open. Technically, in the massless case the external potential is gauged away.

To estimate excitation gaps we develop the phase soli-

ton approach that describes a distortion of the regular lattice of solitons over a length scale greater than its period [as shown schematically in Fig. 1(c)]. An outcome of such a procedure is an effective Lagrangian  $\mathcal{L}_m[\bar{\theta}^0, \bar{\theta}^a]$  for the slow *phase modes* that are constant in the commensurate phase with given density (1), and governs the phase soliton excitation whenever an extra electron is added.

The crucial difference from the case of no external potential is the fact that the saddle point of the phase soliton action  $\mathcal{L}_m[\bar{\theta}^0, \bar{\theta}^a]$  qualitatively depends on whether the electrons are extended over a few potential periods or are tightly bound in the potential minima. We thus distinguish the two regimes of coupling: *weak coupling*

$$\lambda_{\text{ext}}/m \ll l_{\text{fl}} , \quad (2)$$

describing the Bragg diffraction in a Luttinger liquid (Section VII), and that of the *strong coupling*

$$l_{\text{fl}} \ll \lambda_{\text{ext}}/m , \quad (3)$$

equivalent to pinning of the Wigner crystal (Section VIII). These regimes are roughly defined by comparing the mean same-flavor fermion separation  $4\rho^{-1} = \lambda_{\text{ext}}/m$  [cf. Eq. (1)] to the flavor soliton size  $l_{\text{fl}}$  determined self-consistently (more precise definitions will be deferred to Section VI).

In the limit (2) the system “knows” that it is comprised of the particles of the four flavors, and the effects of the fermionic exchange (overlap of the flavor solitons) are important. In Section VII we develop the phase soliton method for the case of the four modes and find the charge and flavor phase soliton excitations. In particular, we show that the flavor excitations are *gapped* (adding electron flavor costs a finite energy of the order of exchange energy), and the corresponding flavor physics is governed by the  $SU(4) \simeq O(6)$  Gross–Neveu model.

In the opposite limit (3) the overlap of the flavor soliton tails of the composite solitons is exponentially small. It is the Coulomb energy that sets the energy scale for the excitation gaps. In this limit, we show in Section VIII that the system is adequately described by an effective theory of *spinless* Dirac fermions interacting via the Coulomb law. Naturally, the regime (3) is the semiclassical limit of the problem. In this limit, in Section IX we draw the phase diagram that has a structure of a devil’s staircase.

### III. THE MODEL

#### A. Nanotube phenomenology

A remarkable feature of Carbon nanotubes is the Dirac symmetry of their electronic spectrum near half-filling<sup>2</sup>. It stems from the semimetallic character of the two-dimensional Carbon monolayer (so-called graphene sheet), whose valence and conduction bands touch each other at the two inequivalent ( $K$  and  $K'$ ) points of the Brillouin zone. These points are separated by a large

wave vector  $K_{\text{BZ}} \sim 1/a_{\text{cc}}$ , where  $a_{\text{cc}} = 0.143$  nm is the length of the Carbon bond. DiVincenzo and Mele<sup>34</sup> made an important observation that the electron spectrum of a graphene sheet near both  $K$  and  $K'$  points in the tight-binding approximation is described in terms of the 2D massless Dirac fermions. A nanotube can be viewed as a wrapped Carbon monolayer. Depending on the NT type, such a wrapping imposes a (quasi)periodic boundary condition on the graphene electrons that may or may not produce an effective mass for the resulting 1D NT fermions. In general, the NT low energy spectrum is controlled by the 1D *massive* Dirac fermions near each of the two Dirac points.<sup>2</sup> In this work we choose the basis (with  $x$  along the tube) in which the Dirac Hamiltonian near the  $K$  or  $K'$  point has the following form:

$$\mathcal{H}_D = -i\hbar v \sigma_3 \partial_x + \Delta_0 \sigma_1 . \quad (4)$$

The Hamiltonian (4) is written in the Weyl basis where the components of the wave function  $\psi = (\psi_R \ \psi_L)^T$  represent the right and left moving particles. Here  $\sigma_{1,3}$  are the Pauli matrices and  $v \approx 8 \cdot 10^7$  cm/s is the NT Fermi velocity. The Hamiltonian (4) yields the Dirac dispersion

$$\epsilon^2(p) = p^2 v^2 + \Delta_0^2 \quad (5)$$

where the momentum  $p \ll \hbar/a_{\text{cc}}$  is measured with respect to the NT Dirac points.

Depending on the NT type, a wide range of values for the Dirac gap  $\Delta_0$  is available<sup>2</sup>.

Semiconducting nanotubes have a large gap

$$\Delta_0^{(\text{semicond.})} = \frac{\hbar v}{3a} \simeq 0.18 \text{ eV}/a_{[\text{nm}]} \quad (6)$$

that is inversely proportional to the NT radius  $a$ .

Metallic NTs can be of the two kinds. There are truly metallic, or the so-called “armchair” NTs which have a zero gap at half-filling,  $\Delta_0 = 0$ . However, a gap

$$\Delta_0 \ll D \quad (7)$$

that is small compared to the 1D bandwidth

$$D = \frac{\hbar v}{a} = 0.53 \text{ eV}/a_{[\text{nm}]} \quad (8)$$

can appear due to the curvature of the 2D graphene sheet in the nominally metallic tube. This gap is inversely proportional to the square of the NT radius, and is numerically given by

$$\Delta_0^{(\text{semimet.})} \approx 10 \text{ meV} \cdot |\cos 3\Theta_{\text{ch}}|/a_{[\text{nm}]}^2 \quad (9)$$

as a function of the NT *chiral angle*  $\Theta_{\text{ch}}$ .<sup>35,36</sup> Even smaller  $\Delta_0$  can be induced in a strictly metallic “armchair” ( $\Theta_{\text{ch}} = \pi/6$ ) tube by applying magnetic field parallel to the NT axis.<sup>37,38</sup>

## B. Coupling to external potential

In the present work we consider the nanotube subject to the external periodic potential which for the purpose of simpler algebra we take to be a harmonic function,

$$U(x) = A \cos k_{\text{ext}} x, \quad k_{\text{ext}} = 2\pi/\lambda_{\text{ext}}. \quad (10)$$

Qualitatively, the results of this work will be valid for any periodic potential realized by the means described in the Introduction.

As mentioned in Section I, realistic values of the period  $\lambda_{\text{ext}}$  are in the  $0.1 - 1 \mu\text{m}$  range. The separation of scales  $k_{\text{ext}} \ll 1/a \ll 1/a_{cc}$  allows us, focussing on the lowest Dirac subband (near half-filling), to discard the coupling between the  $K$  and  $K'$  points in the Brillouin zone since these processes involve momentum transfer  $\sim 1/a_{cc} \gg k_{\text{ext}}$ . Also, in this work we do not consider effects of external magnetic fields. The electrostatic potential (10) couples to the total charge density and does not distinguish between spin polarizations.

As a result, in the absence of electron-electron interactions, we effectively have four ( $2_{\text{spin}} \times 2_{\text{valley}}$ ) decoupled fermion types, which we call ‘‘flavors’’, each described by the same Dirac equation

$$\{\mathcal{H}_D + U(x)\} \psi = \epsilon \psi, \quad (11)$$

where  $\mathcal{H}_D$  is given by Eq. (4).

Coulomb interaction couples the four electron flavors as described below.

## C. Interacting NT electrons in the forward scattering approximation

In what follows we will work in the *forward scattering approximation* established for the nanotubes in Refs. 10 and 11. According to the latter, even in the presence of electron interactions, the two inequivalent Dirac points in the Carbon Brillouin zone (mentioned above in Sec. III A) remain approximately decoupled. As a result, near half filling, nanotubes can be approximately described by the following second-quantized Hamiltonian,

$$\mathcal{H} = \mathcal{H}_0 + \mathcal{H}_{\text{bs}} + \mathcal{H}_{\text{ext}}. \quad (12)$$

The first term  $\mathcal{H}_0$  is the massless Dirac Hamiltonian with the Coulomb interaction between the four fermion flavors:

$$\mathcal{H}_0 = -i\hbar v \int \sum_{\alpha=1}^4 \psi_{\alpha}^{\dagger} \sigma_3 \partial_x \psi_{\alpha} dx + \frac{1}{2} \sum_k \rho_k V(k) \rho_{-k}. \quad (13)$$

Here

$$\psi_{\alpha} = \begin{pmatrix} \psi_{\alpha}^R \\ \psi_{\alpha}^L \end{pmatrix}, \quad 1 \leq \alpha \leq 4 \quad (14)$$

is a two component Weyl spinor of the flavor  $\alpha$ , and

$$\rho(x) = \sum_{\alpha=1}^4 \psi_{\alpha}^{\dagger}(x) \psi_{\alpha}(x) \quad (15)$$

is the total charge density in which we neglected the strongly oscillating components  $\sim e^{\pm 2iK_{\text{BZ}}x}$ , with  $K_{\text{BZ}} \sim 1/a_{cc}$  defining the position of the Dirac points in the Brillouin zone of graphene. For a nanotube of a radius  $a$  placed on a substrate with the dielectric constant  $\epsilon$ , the 1D Coulomb interaction

$$V(k) = \frac{2}{\epsilon+1} V_0(k), \quad (16)$$

where

$$V_0(k) \simeq e^2 \ln [1 + (ka)^{-2}]. \quad (17)$$

In writing the Hamiltonian (13) we have discarded the backscattering and Umklapp processes between the different Dirac points of the graphene Brillouin zone. These processes are small in  $a_{cc}/a \lesssim 0.1$ , with  $a_{cc} = 0.143 \text{ nm}$  being the length of the Carbon bond. The Umklapp amplitude is also small numerically.<sup>12</sup> Since the long range potential (16) does not discriminate between the Carbon sublattices, scattering amplitudes for the fermions of same and opposite chiralities at each Dirac point are equal<sup>10,11</sup>. This naturally leads to the approximation in which electron interaction in Eq. (13) only involves the smooth part (15) of the total electron density.

The second term in the Hamiltonian (12) describes the backscattering between the left and right moving fermions *within* each Dirac point:

$$\mathcal{H}_{\text{bs}} = \Delta_0 \int \sum_{\alpha=1}^4 \psi_{\alpha}^{\dagger} \sigma_1 \psi_{\alpha} dx. \quad (18)$$

The bare gap  $\Delta_0$  can originate due to any of the reasons outlined in Section III A above.

Finally, interaction with the external periodic potential is represented by

$$\mathcal{H}_{\text{ext}} = \int dx \rho U(x), \quad (19)$$

where we use the model potential  $U$  defined in Eq. (10).

The Hamiltonian (12) written in the forward scattering approximation is SU(4) invariant with respect to rotations in the space of the four fermion flavors  $\psi_{\alpha}$ .

## IV. NONINTERACTING ELECTRONS

In the present Section we consider single electron spectrum (11) of a Carbon nanotube in a periodic potential. This simple problem is instructive since it allows us to identify the two regimes of coupling of a NT electron to the external potential in the noninteracting case. They are the limit of nearly free electrons, and the tight-binding limit. To distinguish between them, we compare

the size of the single electron wavefunction  $l_{\text{wf}}$  with the period of the potential  $\lambda_{\text{ext}}$ . These two regimes are to a great extent parallel to, correspondingly, the weak and the strong coupling limits of the fully interacting problem, where one draws the distinction by comparing the quantum sine-Gordon soliton size to  $\lambda_{\text{ext}}$ .

The single particle spectrum has been analyzed in Ref. 24. Below we will study it in detail emphasizing the distinction between the two opposite regimes of coupling. It is convenient to perform a gauge transformation

$$\psi'(x) = e^{-i\bar{A}\sigma_3 \sin k_{\text{ext}}x} \psi(x), \quad (20)$$

where we introduced the dimensionless amplitude

$$\bar{A} = A/\epsilon_0. \quad (21)$$

The kinetic energy scale

$$\epsilon_0 \equiv \hbar k_{\text{ext}}v = hv/\lambda_{\text{ext}} = 3.3 \text{ meV}/\lambda_{\text{ext}} [\mu\text{m}] \quad (22)$$

is the Dirac level spacing in each potential minimum.

After the gauge transformation (20) the Hamiltonian  $\mathcal{H}_D + U(x)$  becomes

$$\mathcal{H}' = -i\hbar v \partial_x \sigma_3 + \Delta_0 \sigma_1 e^{-2i\bar{A}\sigma_3 \sin k_{\text{ext}}x}. \quad (23)$$

Note that due to the Dirac character of the problem, in the Hamiltonian (23) the relative importance of the potential energy (the second term) is governed by the value of the Dirac gap  $\Delta_0$  (rather than the potential amplitude  $A$ ), whereas the kinetic energy (the first term) is  $\mathcal{O}(\epsilon_0)$ .

Due to a variety of the available Dirac gap values  $\Delta_0$ , the coupling of the NT electron to the external potential can be either weak or strong. Consider the eigenvalue problem

$$\mathcal{H}'\psi' = \epsilon\psi' \quad (24)$$

that is periodic in  $\lambda_{\text{ext}}$ . Its solutions are the spinor Bloch states  $\psi_p(x) = u_p(x)e^{ipx}$  with a quasimomentum  $\hbar p$  taking values in the effective Brillouin zone defined by the potential period,  $-k_{\text{ext}}/2 < p < k_{\text{ext}}/2$ . We distinguish between the weak coupling limit (nearly free electrons) and the strong coupling (tight binding) limit by comparing the size  $l_{\text{wf}}$  of the single particle spinor wavefunction  $u_p(x)$  with the period  $\lambda_{\text{ext}}$  of the potential. The length scale  $l_{\text{wf}}$  in general depends on the quasimomentum  $p$ , on the backscattering  $\Delta_0$  and on the profile and strength of the external potential.

In the limit of *nearly free electrons*

$$\lambda_{\text{ext}} \ll l_{\text{wf}}. \quad (25)$$

In this case the electron wave functions are close to plane waves.

Note that in the *massless* case of  $\Delta_0 = 0$ ,  $l_{\text{wf}} = \infty$ , and the external potential has no effect since it is gauged away. This is a manifestation of the fact that the scalar external potential does not mix massless Dirac branches

whose wave functions have a spinor structure. The other way of understanding it is that, in agreement with the above discussion, the potential energy scale is determined by the backscattering  $\Delta_0$ , vanishing when  $\Delta_0 = 0$ .

In the presence of small backscattering, diffraction on the periodic potential results in mixing between the left and right moving states of the Dirac spectrum at particular values

$$p_m = \pm \frac{m}{2} k_{\text{ext}}, \quad m = \pm 1, \pm 2, \dots \quad (26)$$

of the electron quasimomentum, opening minigaps in the single particle spectrum. Perturbative treatment of the potential term yields the minigaps<sup>24</sup>

$$\Delta_m^{(0)}(\bar{A}) = \Delta_0 |J_m(2\bar{A})| \quad (27)$$

that open at the energy values  $\epsilon_m = m\epsilon_0/2$ . The superscript (0) in Eq. (27) relates to the noninteracting case. Minigaps (27) oscillate as a function of the potential amplitude  $A$  and vanish for particular values of  $A$  corresponding to zeroes of the Bessel functions  $J_m$ .

The opposite regime is the *strong coupling*, or the *tight-binding limit*

$$l_{\text{wf}} \leq \lambda_{\text{ext}}, \quad (28)$$

in which case the external potential localizes the semiclassical Dirac electrons (holes) in its minima (maxima). In this case the corresponding minigaps become larger than the subbands. The spectrum can be obtained by solving the problem (24) numerically by the transfer matrix. For an illustration, in Fig. 2 we plot the spectrum for the borderline case  $\Delta_0 = \epsilon_0$  in which the potential and kinetic energy in the Hamiltonian (23) are of the same order. Similarly to the nearly free electron limit, the energy gaps oscillate as a function of  $A$  and vanish

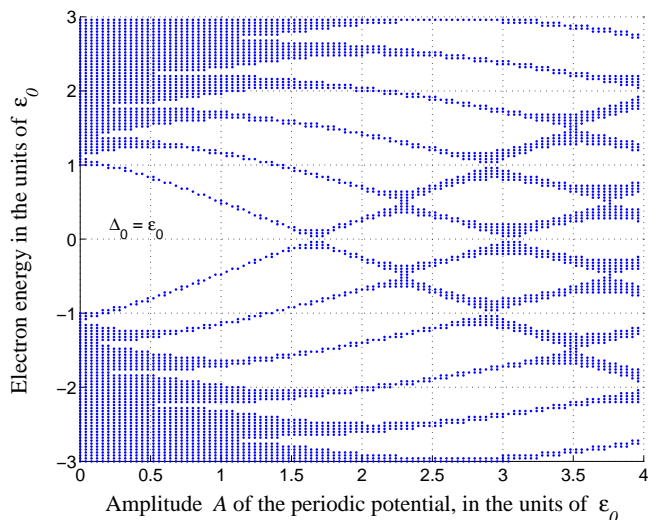


FIG. 2: Single electron spectrum for the nanotube in the presence of the external potential (10) for the case  $\Delta_0 = \epsilon_0$

at certain amplitude values. The spectrum also has a characteristic Dirac  $\epsilon \rightarrow -\epsilon$  symmetry.

Fig. 2 suggests that even for the case  $\Delta_0 = \epsilon_0$  minigaps occupy most of the spectrum when  $A \sim \epsilon_0$ . In this case the electron dispersion in each miniband is almost flat. This corresponds to electrons and holes being localized in the minima and maxima of the external potential correspondingly, with an exponentially suppressed tunneling between the adjacent potential wells.

In Appendix A we show that the limit (28) of the exponentially suppressed inter-well tunneling holds whenever

$$\left(\frac{\Delta_0}{\epsilon_0}\right)^{-1} < \frac{A}{\epsilon_0} < \left(\frac{\Delta_0}{\epsilon_0}\right)^c, \quad \Delta_0 > \epsilon_0, \quad (29)$$

where the exponent  $c = 3$  for tunneling from an energy level close to the bottom of the potential, and  $c = 2$  for tunneling from a level far from the minimum.

Increasing the potential amplitude  $A$  beyond  $\Delta_0/\epsilon_0^{c-1}$  actually *enhances* the tunneling amplitude between the particle and hole continua. This is reflected in Fig. 2 by wider minibands for  $A > \epsilon_0$ . Indeed, an increase in  $A$  makes the tunneling barrier through the Dirac gap  $2\Delta_0$  shorter, and reduces the action under the barrier. The other way of understanding the apparent delocalization of the wave functions for large  $A$  is to notice that large

potential amplitude results in strong oscillations of the potential term in Eq. (23). These oscillations effectively average this term to zero in the limit  $A \rightarrow \infty$ , in which case the minigaps become small as  $A^{-1/2}$ . The latter follows from the large- $A$  asymptotic behavior of the Bessel functions for the weak coupling minigaps (27) that become valid in this limit.

## V. BOSONIZATION

We bosonize<sup>10,11,13,14,24</sup> the Hamiltonian (12) by virtue of the massive Thirring – quantum sine-Gordon duality,<sup>22,23</sup> by representing the fermionic operators (14) as nonlocal combinations of bose fields

$$\psi_\alpha = \frac{1}{\sqrt{2\pi a}} e^{i\Theta_\alpha}. \quad (30)$$

The conjugate momenta

$$\Pi_\alpha = \frac{1}{\pi v} \partial_t \Theta_\alpha \quad (31)$$

obey the usual canonical relations  $[\Pi_\alpha(x), \Theta_\beta(y)]_- = -i\delta_{\alpha\beta} \delta(x-y)$ . As a result we obtain the Lagrangian

$$\mathcal{L} = \frac{\hbar v}{2\pi} \int dx \sum_{\alpha=1}^4 \left( \frac{1}{v^2} (\partial_t \Theta_\alpha)^2 - (\partial_x \Theta_\alpha)^2 \right) - \frac{1}{2} \sum_q \rho_{-q} V(q) \rho_q - \int dx \left( \frac{\Delta_0}{\pi a} \sum_{\alpha=1}^4 \cos 2\Theta_\alpha + \rho(x) U(x) \right), \quad (32)$$

where the total charge density (1) in terms of the bosonic variables is given by

$$\rho(x) = \sum_{\alpha=1}^4 \rho_\alpha = \sum_{\alpha=1}^4 \frac{1}{\pi} \partial_x \Theta_\alpha. \quad (33)$$

The Lagrangian (32) corresponds to the sine-Gordon Hamiltonian for the four interacting bosonic fields  $\Theta_\alpha$ ,

$$\mathcal{H}_{\text{SG}}[\Theta_\alpha] = \frac{\hbar v}{\pi} \int dx \left\{ \frac{1}{2} \sum (\partial_x \Theta_\alpha)^2 + \frac{K-1}{8} \left( \sum \partial_x \Theta_\alpha \right)^2 + \frac{1}{4} g_0 \sum \cos 2\Theta_\alpha + \frac{1}{\hbar v} \sum \partial_x \Theta_\alpha \cdot (U(x) - \mu) \right\}. \quad (34)$$

Here the coupling (bare backscattering)

$$g_0 = \frac{4\Delta_0}{\hbar v a} = \frac{4}{a^2} \frac{\Delta_0}{D}, \quad (35)$$

where  $D$  is the bandwidth (8),  $\mu$  is the chemical potential calculated from the half filling, and the charge stiffness

$$K_q = 1 + 4\nu V(q), \quad \nu = \frac{1}{\pi \hbar v}. \quad (36)$$

Below we drop the (irrelevant) logarithmic dependence of the stiffness  $K_q$  on the momentum, assuming a constant

value  $K \equiv K_{q \sim 1/l_{\text{ch}}}$ , where  $l_{\text{ch}} \sim l_s$  is the charge soliton size (screening length for the Coulomb interaction). Using  $e^2/\hbar v \simeq 2.7$  we estimate  $K \simeq 40$  for  $l_{\text{ch}} \sim 1 \mu\text{m}$  for the stand-alone tube;  $K \simeq 10$  for the tube placed on a substrate with a dielectric constant  $\epsilon = 10$ .

We shift the displacement fields

$$\Theta_\alpha(x) \rightarrow \Theta_\alpha(x) - \frac{1}{\hbar v} \int^x K^{-1} (U - \mu) dx' \quad (37)$$

[gauge transforming the fermion operators (20)]. The transformed Hamiltonian (34) is

$$\mathcal{H}'_{\text{sG}}[\Theta_\alpha] = \frac{\hbar v}{\pi} \int dx \left\{ \frac{1}{2} \sum (\partial_x \Theta_\alpha)^2 + \frac{K-1}{8} \left( \sum \partial_x \Theta_\alpha \right)^2 + \frac{1}{4} g_0 \sum_{\alpha=1}^4 \cos \left( 2\Theta_\alpha + 2\tilde{\mu} k_{\text{ext}} x - 2\tilde{A} \sin k_{\text{ext}} x \right) \right\}, \quad (38)$$

where the dimensionless quantities

$$\tilde{A} = \frac{A}{K\epsilon_0}, \quad \tilde{\mu} = \frac{\mu}{K\epsilon_0} \quad (39)$$

are introduced in a way similar to that of Eq. (21), with the energy scale  $\epsilon_0$  defined in Eq. (22). The difference between Eqs. (39) and (21) is in additional *screening* (by a factor of  $1/K$ ) of external fields  $U(x)$  and  $\mu$  by the interacting NT system.

When  $g_0 = 0$ , the fermion density  $m$  varies continuously with  $\tilde{\mu}$  as

$$m = 2\tilde{\mu}. \quad (40)$$

In this case the system is a compressible scale-invariant Tomonaga-Luttinger liquid of the four flavors regardless of how strong the electron-electron repulsion is.<sup>39</sup>

We diagonalize the Gaussian part of the action by the unitary transformation<sup>13,24</sup>

$$\begin{pmatrix} \Theta_1 \\ \Theta_2 \\ \Theta_3 \\ \Theta_4 \end{pmatrix} = \frac{1}{2} \begin{pmatrix} 1 & 1 & 1 & 1 \\ 1 & -1 & 1 & -1 \\ 1 & -1 & -1 & 1 \\ 1 & 1 & -1 & -1 \end{pmatrix} \begin{pmatrix} \theta^0 \\ \theta^1 \\ \theta^2 \\ \theta^3 \end{pmatrix}. \quad (41)$$

In the new variables the total charge density (33) reads

$$\rho(x) = \frac{2}{\pi} \partial_x \theta^0. \quad (42)$$

Gauge transformation (37) leaves  $\theta^a$  intact, and shifts

$$\theta^0 \rightarrow \theta^0 - \frac{2}{\hbar v} \int^x K^{-1} (U - \mu) dx'. \quad (43)$$

Using the identity

$$\sum_{\alpha=1}^4 \cos 2\Theta_\alpha = 4\mathcal{F}(\theta^0, \theta^a), \quad (44)$$

where

$$\mathcal{F}(\theta^0, \theta^a) = \cos \theta^0 \cdot \prod_{a=1}^3 \cos \theta^a + \sin \theta^0 \cdot \prod_{a=1}^3 \sin \theta^a, \quad (45)$$

as a result we obtain the Lagrangian<sup>13,24</sup>

$$\mathcal{L}' = \mathcal{L}_0 + \mathcal{L}_{\text{bs}} \quad (46)$$

describing one stiff charge mode and three soft flavor modes, where

$$\begin{aligned} \mathcal{L}_0 &= \frac{\hbar v}{2\pi} \int dx \left( \frac{1}{v^2} (\partial_t \theta^0)^2 - K (\partial_x \theta^0)^2 \right) \\ &+ \frac{\hbar v}{2\pi} \int dx \sum_{a=1}^3 \left( \frac{1}{v^2} (\partial_t \theta^a)^2 - (\partial_x \theta^a)^2 \right), \end{aligned} \quad (47)$$

$$\mathcal{L}_{\text{bs}} = -\frac{\hbar v g_0}{\pi} \int dx \mathcal{F}(\theta^0 + 2\tilde{\mu} k_{\text{ext}} x - 2\tilde{A} \sin k_{\text{ext}} x, \theta^a) \quad (48)$$

The Gaussian Lagrangian  $\mathcal{L}_0$  describes three flavor modes that move with velocity  $v$ , and one charge mode that has a strongly enhanced velocity

$$\bar{v} = K^{1/2} v. \quad (49)$$

This is a manifestation of the separation between charge and flavor in a strongly interacting system described by the Hamiltonian  $\mathcal{H}_0$ . The interaction term (48) becomes relevant at certain electron densities and is responsible for incompressible states.

Note that the Lagrangians (32) and (46) are SU(4) invariant, as is the original Hamiltonian  $\mathcal{H}$ . This invariance is not explicit in the adapted notation. It will manifest itself below at the level of renormalization.

## VI. PHASE SOLITON APPROACH FOR NANOTUBE ELECTRONS

### A. Saddle point: No external potential

Consider first the strongly interacting [ $K \gg 1$ ] NT electrons in the case of no external potential. At half filling, this system is described by the Lagrangian (46) with  $A = 0$  and  $\mu = 0$ . By raising the chemical potential above the gap one adds a single electron with a particular flavor. As it will be necessary below to find the scaling laws, and for consistency of the presentation, we are going to describe such an excitation in detail, following the approach of Levitov and Tsel'ik.<sup>13</sup>

As shown in Ref. 13, the lowest energy charged excitation is a combination of solitons of the charge and flavor modes (a *composite soliton*) characterized by the presence of the two length scales: flavor  $l_{\text{fl}}$  and charge  $l_{\text{ch}} \sim K^{1/2} l_{\text{fl}}$ , so that  $l_{\text{ch}} \gg l_{\text{fl}}$ . In such an excitation the soft flavor modes  $\theta^a$  optimize the effective potential for the stiff charge mode  $\theta^0$  and add a particular flavor to an electron. In other words, flavor becomes bound to charge by the non-linear term (48). According to the transformation (41), adding an electron of any flavor (*i.e.* changing a particular  $\Theta_\alpha$  by  $\pi$ ) results in a configuration in which all the fields  $\theta^0, \theta^a$  change by  $\pm\pi/2$ . Since  $l_{\text{ch}} \gg l_{\text{fl}}$  in the limit of the large stiffness  $K \gg 1$ , solitons of the flavor modes  $\theta^a$  can be viewed as infinitely sharp steps on the scale of  $l_{\text{ch}}$ . As suggested in Ref. 13, such a sharp “switching” of the flavor modes can optimize the potential term  $\mathcal{L}_{\text{bs}}$  in the total Lagrangian (46) by providing an effective potential  $\propto g\mathcal{F}_{\text{cl}}(\theta^0)$  for a soliton of the stiff charge mode, where  $g$  is the renormalized value

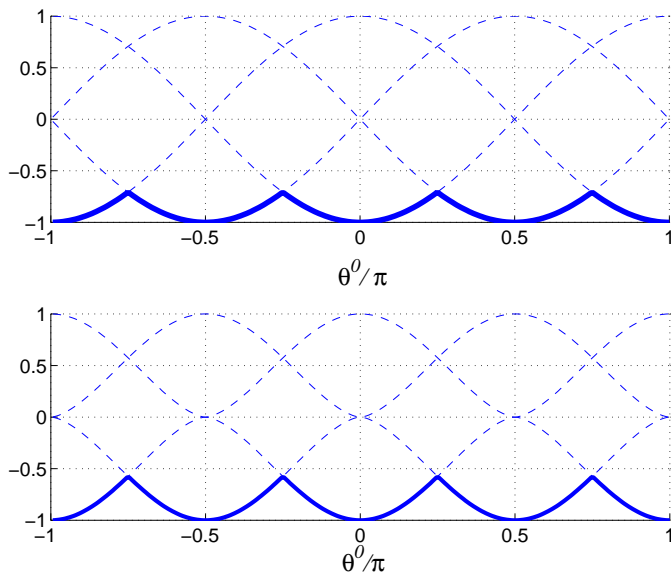


FIG. 3: Classical  $\bar{\mathcal{F}}_{\text{cl}}(\theta^0)$  (top) and renormalized  $\bar{\mathcal{F}}(\theta^0)$  (bottom) effective potentials (shown in bold) for the charge mode in the case of  $K \gg 1$ , Eqs. (50) and (53)

for the backscattering (35), and the function

$$\bar{\mathcal{F}}_{\text{cl}}(\theta^0) = \min_{\{\theta^a\}} \mathcal{F}(\theta^a, \theta^0) = \min \{ \cos \theta^0, \sin \theta^0 \} \quad (50)$$

is shown in the top panel of Fig. 3. For that the flavor modes  $\theta^a$  should switch at the point when  $\theta^0$  is changed by  $\pi/4$ , in which case the *classical* soliton of the charge mode is of the form<sup>13</sup>

$$\theta_{\text{cl}}^0(x) = \begin{cases} 2 \cos^{-1} \tanh(u - x/l_{\text{ch}}), & x < 0, \\ \frac{\pi}{2} - 2 \cos^{-1} \tanh(u + x/l_{\text{ch}}), & x > 0, \end{cases} \quad (51)$$

where  $l_{\text{ch}} = (K/g)^{1/2}$  and  $\tanh u = \cos \pi/8$ .

Authors of Ref. 13 have included effects of quantum fluctuations of the soft neutral sector in the scaling of the coupling  $g$ . However, in the adiabatic approximation  $l_{\text{ch}} \gg l_{\text{fl}}$ , the potential (50) is slow on the scale  $a < l < l_{\text{fl}}$  on which quantum fluctuations of the fields  $\theta^a$  are significant. The RG treatment (Sec. VI E below) results in the universal exponent

$$\gamma = 8/5 \quad (52)$$

of the *whole* potential term (50).<sup>40</sup> As a result, strictly speaking, the effective potential for the charge sector should be corrected by the scaling (52):

$$\begin{aligned} V_{\text{charge}} &= g \bar{\mathcal{F}}(\theta^0), \\ \bar{\mathcal{F}}(\theta^0) &= -(-\bar{\mathcal{F}}_{\text{cl}}(\theta^0))^\gamma, \end{aligned} \quad (53)$$

where the renormalized backscattering amplitude

$$g \simeq \frac{1}{a^2} \left( \frac{\Delta_0}{D} \right)^\gamma \quad (54)$$

and the cutoff  $D$  is defined in Eq. (8). The function  $\bar{\mathcal{F}}(\theta^0)$  is plotted in the lower panel of Fig. 3.

It can be shown<sup>41</sup> that the difference between the potentials (53) and (50) is qualitatively unimportant for the further discussion. It brings about only a numerical factor (order unity) for the charge soliton energy. Indeed, although the exact analytic form for the charge mode soliton with the potential term (53) is unavailable, it is qualitatively similar to the classical soliton (51). Approximating the potential (53) by the piecewise-quadratic function, the charge mode soliton is

$$\theta_{\text{quad}}^0(x) = \begin{cases} \frac{\pi}{4} e^{x/l_{\text{ch}}}, & x < 0, \\ \frac{\pi}{2} - \frac{\pi}{4} e^{-x/l_{\text{ch}}}, & x > 0, \end{cases} \quad (55)$$

with a charge soliton size

$$l_{\text{ch}} = (K/\gamma g)^{1/2} \quad (56)$$

a factor  $\approx 1.26$  shorter compared to that in Eq. (51).

The important message of this treatment is that in the presence of the Coulomb repulsion the soft neutral modes adjust themselves in a *saddle-point fashion* [with  $K \gg 1$  playing the role of  $\hbar^{-1}$ ] to provide an effective potential (53) for the stiff charge mode. This effective potential has a period  $\pi/2$  that is four times smaller than that of the potential (48) with *fixed*  $\theta^a$ . Indeed, the lowest harmonic in the Fourier expansion

$$\bar{\mathcal{F}}(\theta^0) = \text{const.} + \sum_{n=1}^{\infty} f_n \cos(4n\theta^0) \quad (57)$$

is  $\cos 4\theta^0$ . The purpose of this period reduction is to lower the Coulomb energy by splitting the  $\theta^0 \rightarrow \theta^0 + 2\pi$  excitation that carries charge  $4e$  [according to Eq. (42)] and is a flavor singlet, into four subsequent excitations each carrying a single fermion (of a particular flavor).

As a result, when studying the Wigner crystal regime where the charge sector dominates, we will substitute the potential  $\bar{\mathcal{F}}(\theta^0)$  by its lowest harmonic from Eq. (57),

$$\bar{\mathcal{F}}(\theta^0) \approx f_1^* \cos 4\theta^0 \quad (58)$$

with the coefficient  $f_1^* = \mathcal{O}(1)$  chosen in such a way that the energy of the charge soliton for the true potential (53) is equal to that for the potential (58). In this case the charge soliton takes the approximate form

$$\theta_{\text{approx}}^0(x) = \frac{1}{2} \cos^{-1} \tanh(-x/l_{\text{ch}}') \quad (59)$$

with the rescaled size  $l_{\text{ch}}' = \frac{1}{4}(K/f_1^*g)^{1/2} \propto l_{\text{ch}}$ . Approximation (58) is adequate in the strong coupling limit (Section VIII). It yields the appropriate scaling laws, provides a way to calculate excitation gaps, and results in the devil's staircase in the classical limit (Section IX). The error of this approximation is in the overall coefficient in the renormalized excitation gaps, that cannot be reliably determined from bosonization anyway due to dependence on the somewhat arbitrary 1d bandwidth  $D$ .

By raising the chemical potential  $\mu$  above the (renormalized) charge gap  $\Delta$  one obtains a compressible train of composite solitons. For small electron density, when the overlap of flavor soliton cores is exponentially small, such a configuration is a one-dimensional Wigner crystal. Composite soliton centers correspond to classical positions of the electrons, and the exchange effects due to overlap between flavor solitons are negligible. Coulomb interaction (described by overlap of the charge solitons) maintains quasi-long range order in a finite system. In a real system the Coulomb repulsion is never infinitely long range, it is cut off at some screening length  $l_s$  (e.g. tube length or the distance to the metallic gate). The length  $l_s$  sets the scale for the charge stiffness  $K = K_{ql_s} \simeq 1$ . At higher density the flavor soliton cores begin to overlap and exchange effects become important. At large density  $\rho l_s \gg 1$  the system enters the regime of the scale-invariant Tomonaga-Luttinger liquid, in which case the non-linear term of the action (46) becomes irrelevant. In this case the chemical potential is much greater than the Dirac gap, so that the electronic dispersion is approximately linear, corresponding to fully extended excitations. Since there is no phase transition in one dimension, the transition between the Wigner crystal and the Tomonaga-Luttinger liquid occurs smoothly, in a crossover fashion, as described above.

### B. Incompressible states of the classical bose fields

Let us add the external periodic potential (10) to the *classical* Hamiltonian (34). Our purpose is to demonstrate that the *saddle point* of the system (46) already captures many important features of the real physical system. Consider the simplest fractional case of  $m = 1/2$ , corresponding to the chemical potential  $\tilde{\mu} = 1/4$  [cf. Eq. (40)]. This is an incompressible classical configuration in which the solitons of the fields  $\Theta_\alpha$  occupy every other potential minimum, as shown in Fig. 4. This Figure is a result of a numerical minimization of the Hamiltonian (34) with respect to the fields  $\Theta_\alpha$ . For any rational density  $m = p/q$  the period of each field  $\Theta_\alpha$  is  $q\lambda_{\text{ext}}$ , with  $q = 2$  in Fig. 4. The *total* density  $m_{\text{tot}} = 2$  is integer, hence the charge density period coincides with that of  $U(x)$ . In the absence of  $U(x)$ , all the  $\Theta_\alpha$  solitons would be equally separated from each other due to the Coulomb repulsion. The finite  $U$  configuration shown in Fig. 4 is a result of an interplay between the mutually repelling solitons and a confining periodic potential. Fermionic exchange of the original problem (12) is manifest in the fact that solitons of the same flavor are located in different potential minima.

In what follows we will find the energy cost of a charged excitation in *quantum-mechanical* analogs of the commensurate classical soliton states. For that we will develop the analytical method that generalizes the phase soliton method to the case of the four modes and takes into account quantum fluctuations.

### C. Phase soliton method

Let us now outline the way to analytically study the ground state and excitation gaps for the commensurate states characterized by the density (1) in which  $m$  can be either integer or a simple fraction  $m = p/q$ . Starting from the bosonized Lagrangian (46) with the chemical potential corresponding to the density  $m$  according to Eq. (40), one expands the bose-fields in powers of backscattering  $g_0$  as

$$\begin{aligned} \theta^0 &= \bar{\theta}^0 + \theta^{0(1)} + \dots + \theta^{0(n)} + \dots, \\ \theta^a &= \bar{\theta}^a + \theta^{a(1)} + \dots + \theta^{a(n)} + \dots, \\ \theta^{0(n)} &= \mathcal{O}(g_0^n), \quad \theta^{a(n)} = \mathcal{O}(g_0^n), \end{aligned} \quad (60)$$

and then finds the effective Lagrangian

$$\mathcal{L}_m[\bar{\theta}^0, \bar{\theta}^a] = \mathcal{L}_0[\bar{\theta}^0, \bar{\theta}^a] + \mathcal{L}_m^{\text{int}}[\bar{\theta}^0, \bar{\theta}^a] \quad (61)$$

for the phase modes  $\bar{\theta}^0$  and  $\bar{\theta}^a$  to the lowest order in  $g_0$ . Here the first term is the Gaussian Lagrangian (47) as a function of the slow phase modes, and the potential energy  $\mathcal{L}_m^{\text{int}}$  is of the order  $g_0^q$  (before integrating over quantum fluctuations).

From the Lagrangian  $\mathcal{L}_m[\bar{\theta}^0, \bar{\theta}^a]$  one finds the commensurate ground state in which the phase modes  $\bar{\theta}^0$  and  $\bar{\theta}^a$  are constant. An excitation over such a ground state is a *composite phase soliton* of the slow modes  $\bar{\theta}^0(x)$ ,  $\bar{\theta}^a(x)$ . It can be found as a saddle point of the Lagrangian  $\mathcal{L}_m[\bar{\theta}^0, \bar{\theta}^a]$  in a way similar to that described above in Sec. VIA. Its energy will in general come from both the charge and the flavor sectors. Usually, due to  $K \gg 1$ ,

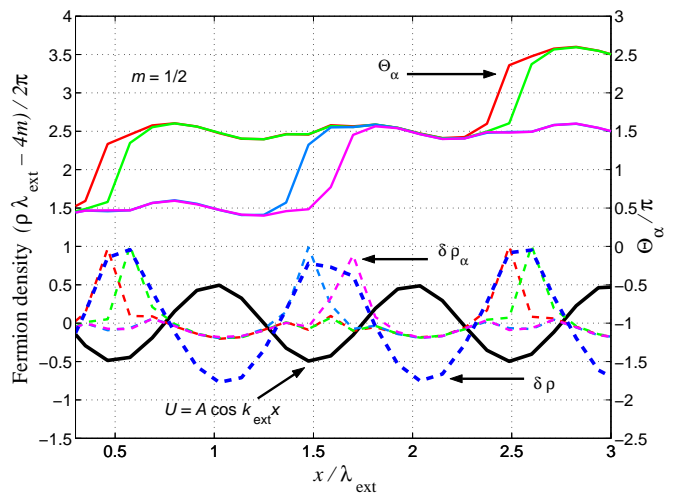


FIG. 4: Classical ground state of the Hamiltonian (34) for the fractional density  $m = 1/2$ . Solitons of the fields  $\Theta_\alpha$  (solid lines) as a result of numerical minimization of Eq. (34) for  $\tilde{\mu} = 1/4$ ,  $K = 10$ ,  $g_0 = 48k_{\text{ext}}^2$ ,  $A = K\epsilon_0$ . Dashed lines are the corresponding partial flavor densities  $\delta\rho_\alpha = \rho_\alpha - m/\lambda_{\text{ext}}$  counted from their average  $m/\lambda_{\text{ext}}$ . Bold dashed line is the total charge density counted from the total average  $4m/\lambda_{\text{ext}}$ . Note the period doubling for the fields  $\Theta_\alpha(x)$ .

the excitation gap will be dominated by the energy of the charge soliton  $\bar{\theta}^0(x)$ . However, we will show that in the weak coupling limit (2) of the delocalized flavor solitons, exchange becomes important in stabilizing excitation gaps at certain instances when the charge gap accidentally closes (Section VII).

#### D. Weak vs. strong coupling

Below we will demonstrate that the NT electron system has two qualitatively different regimes of coupling to external potential that are determined by a choice of the saddle point of the Lagrangian  $\mathcal{L}_m[\bar{\theta}^0, \bar{\theta}^a]$ . To illustrate this point, we consider the simplest phase mode Lagrangian, namely the one for the *integer* density  $m$ , in which case the decomposition (60) is trivial since it contains just one term for each mode. Hence  $\mathcal{L}_m[\bar{\theta}^0, \bar{\theta}^a]$  is precisely the Lagrangian (46) written as a function of  $\theta^{0,a} = \bar{\theta}^{0,a}$  with the chemical potential  $\tilde{\mu}$  given by Eq. (40). [This integer- $m$  case is also considered in Sec. VII A below.]

To define the regimes of coupling we need the size  $l_{\text{fl}}$  of the phase soliton  $\bar{\theta}^a(x)$  of the flavor sector (“flavor scale”). For now we assume that  $l_{\text{fl}}$  is known. The scale  $l_{\text{fl}}$  will be obtained self-consistently as a result of integrating over the quantum *fluctuations* (performed for different cases in Sections VI E, VII and VIII).

##### *Weak coupling*

In the weak coupling regime the flavor soliton tails that correspond to fermions of the *same* flavor overlap. Physically, it means that the system “knows” that it is composed of the particles of different flavor since the role of exchange is important. An extreme example of this regime is a non-interacting system in which fermions of the same flavor effectively repel due to the Pauli principle, whereas fermions of different flavors do not notice each other.

Technically, the weak coupling regime is characterized by the *slow* “switching” of the flavor modes  $\theta^a$  (described in Sec. VI A above) on the scale on which the phase of the charge part of the potential energy  $\mathcal{L}_m^{\text{int}}[\bar{\theta}^0, \bar{\theta}^a]$  in the Lagrangian (61) changes by  $2\pi$ . For integer  $m$ , the potential energy is just the nonlinear term (48) written as a function of the slow modes  $\bar{\theta}^0, \bar{\theta}^a$ . Thus we demand

$$\begin{aligned} mk_{\text{ext}}l_{\text{fl}} &\gg 2\pi, \\ 2\tilde{A}\sin k_{\text{ext}}l_{\text{fl}} &\gg 2\pi. \end{aligned} \quad (62)$$

The first condition in Eq. (62) requires the flavor excitation to be extended on the scale of the distance  $4\rho^{-1} = \lambda_{\text{ext}}/m$  between same-flavor fermions. It is equivalent to Eq. (2). The meaning of the second condition will be made more clear below. Practically, Eq. (62) is equivalent to (2) when the potential amplitude is not

large,  $A < K\hbar v/l_{\text{fl}}$ . The weak coupling limit (62) results in the following approximation for the energy (48):

$$\begin{aligned} &\mathcal{F}\left(\bar{\theta}^0 + mk_{\text{ext}}x - 2\tilde{A}\sin k_{\text{ext}}x, \bar{\theta}^a\right) \\ &\approx J_m(2\tilde{A})\mathcal{F}(\bar{\theta}^0, \bar{\theta}^a) \rightarrow J_m(2\tilde{A})\bar{\mathcal{F}}_{\text{cl}}(\bar{\theta}^0). \end{aligned} \quad (63)$$

Here we discarded spatially oscillating terms (in other words, averaged  $\mathcal{F}$  over the period  $\lambda_{\text{ext}}$ ), and denoted by the arrow the soft mode “switching” that produced the “optimized” potential (50). The procedure (63) as written is allowed for the integer density  $m$ . In the case when the density  $m = p/q$  is a simple fraction one needs to utilize the phase soliton approach to find the effective potential of order  $g_0^q$  and then perform a procedure analogous to Eq. (63).

The weak coupling limit is considered in Sec. VII A for integer  $m$  and in Sec. VII B for the simplest fractional density  $m = 1/2$ .

##### *Strong coupling*

In the opposite limit (3) the Coulomb interaction dominates effects of the fermionic exchange. In this regime the system “forgets” its four-flavor nature, and effectively behaves as that of spinless Dirac fermions with the total density (1). Technically, the soft mode “switching” (denoted by the arrow below) occurs *before* averaging over the period of the potential,

$$\begin{aligned} &\mathcal{F}\left(\bar{\theta}^0 + mk_{\text{ext}}x - 2\tilde{A}\sin k_{\text{ext}}x, \bar{\theta}^a\right) \\ &\rightarrow \bar{\mathcal{F}}\left(\bar{\theta}^0 + mk_{\text{ext}}x - 2\tilde{A}\sin k_{\text{ext}}x\right) \\ &= f_1 \cos\left(4\bar{\theta}^0 + m_{\text{tot}}k_{\text{ext}}x - 8\tilde{A}\sin k_{\text{ext}}x\right) \\ &+ f_2 \cos\left(8\bar{\theta}^0 + 2m_{\text{tot}}k_{\text{ext}}x - 16\tilde{A}\sin k_{\text{ext}}x\right) + \dots \\ &\approx f_1^* \cos\left(4\bar{\theta}^0 + m_{\text{tot}}k_{\text{ext}}x - 8\tilde{A}\sin k_{\text{ext}}x\right). \end{aligned} \quad (64)$$

Here the Fourier coefficients  $f_n$  are defined in Eq. (57), and in the last line we used the approximation (58). Note the dependence of the resulting potential energy on the *total density*  $m_{\text{tot}} = 4m$ . The condition for the saddle point (64) is

$$\begin{aligned} mk_{\text{ext}}l_{\text{fl}} &< 2\pi, \\ 2\tilde{A}\sin k_{\text{ext}}l_{\text{fl}} &< 2\pi. \end{aligned} \quad (65)$$

In Section VIII we will study the effective potential obtained in Eq. (64) in detail. We will show that after the neutral fields  $\bar{\theta}^a$  are integrated out, the resulting Lagrangian for the charge mode can be re-fermionized. It will describe a *single* fermionic mode with the total density (1) and renormalized backscattering, that interacts with the external periodic potential.

Now let us clarify the meaning of the second condition in Eqs. (62) and (65). Increasing the potential amplitude  $A$  beyond  $K\hbar v/l_{\text{fl}}$  makes the external potential alter the

flavor correlations that develop on the scale  $l_{\text{fl}}$ . This can draw the system into the weak coupling limit (62). This situation is similar to the non-interacting case considered in Section IV above. In both cases, a very strong potential amplitude averages out the effect of the external potential.

### E. Effect of quantum fluctuations

To illustrate the integration over the quantum fluctuations, let us renormalize the charge gap  $\Delta$  for the case of a half-filled nanotube in the absence of external potential (generalization for the case with the external potential presents no problem). The saddle point for this case was described in Sec. VI A above. Quantum fluctuations of the neutral modes are described by the Lagrangian of the form [cf. Eq. (46)]

$$\begin{aligned} \mathcal{L}[\theta^a] = & \frac{\hbar v}{2\pi} \int dx \sum_{a=1}^3 \left( \frac{1}{v^2} (\partial_t \theta^a)^2 - (\partial_x \theta^a)^2 \right) \\ & - \hbar v \int dx \tilde{g} \prod_{a=1}^3 \cos \theta^a + (\cos \leftrightarrow \sin), \end{aligned} \quad (66)$$

where  $\tilde{g} = (g_0/\pi) \cos \theta^0$  and  $g_0$  is proportional to the bare NT gap  $\Delta_0$  [Eq. (35)]. Adiabaticity of the charged mode at  $K \gg 1$  ensures that  $\tilde{g} \simeq \text{const.}$  on the length scales  $a < l < l_{\text{fl}}$  where quantum fluctuations of the flavor modes are relevant. With each neutral field in the product in Eq. (66) contributing to the scaling dimension by 1/4, flavor fluctuations result in the net scaling dimension

$$\gamma_0 = \frac{3}{4} \quad (67)$$

for the potential term in Eq. (66), yielding the scaling

$$\tilde{g}(l) = \tilde{g}(a) \left( \frac{l}{a} \right)^{-\gamma_0}, \quad (68)$$

where  $l$  is the RG scale and  $a$  is the tube radius. Since  $\gamma_0 < 2$  the coupling  $\tilde{g}$  is relevant and grows. The flow (68) stops on the scale  $l = l_{\text{fl}}$  on which the potential energy becomes comparable to the kinetic energy of the flavor sector, since the perturbative RG yields the law (68) only while the *renormalized* coupling  $\tilde{g}(l)$  stays small.<sup>42</sup> For the larger scales  $l > l_{\text{fl}}$  the potential energy dominates and the problem becomes classical.

The scale  $l_{\text{fl}}$  has a twofold meaning.

First, it is the *correlation length* for the flavor modes. It can be estimated self-consistently from the balance of kinetic and potential terms

$$\tilde{g}(l_{\text{fl}}) \simeq \frac{1}{l_{\text{fl}}^2}. \quad (69)$$

Beyond  $x \simeq l_{\text{fl}}$  the correlation functions of the  $\theta^a$  fields decay exponentially (rather than in a power-law fashion).

From Eqs. (68) and (69) we obtain the renormalized potential (53) for the charge mode with the renormalized coupling (54) and the scaling exponent (52),

$$\gamma = \frac{2}{2 - \gamma_0}. \quad (70)$$

The second meaning of the scale  $l_{\text{fl}}$  is the *size of the flavor soliton*. Indeed, Eq. (69) is exactly the way to estimate the soliton size of the fields  $\theta^a$  in a sine-Gordon model [Eq. (66) with the renormalized coupling  $\tilde{g} = \tilde{g}(l_{\text{fl}})$ ].

Since the charge sector is stiff, the excitation gap  $\Delta$  is dominated by the charge soliton energy. The latter can be now estimated classically from the effective charge mode Lagrangian

$$\begin{aligned} \mathcal{L}_{\text{charge}} = & \frac{\hbar v}{\pi} \int dx \left( \frac{1}{2v^2} (\partial_t \theta^0)^2 - \frac{K}{2} (\partial_x \theta^0)^2 - V_{\text{charge}} \right) \\ \approx & \frac{\hbar v}{\pi} \int dx \left( \frac{1}{2v^2} (\partial_t \theta^0)^2 - \frac{K}{2} (\partial_x \theta^0)^2 - g f_1^* \cos 4\theta^0 \right) \end{aligned} \quad (71)$$

where we used the saddle point approximation (53), (54) and (58) outlined in Sec. VI A above. The effective Lagrangian (71) yields the gap<sup>13,24</sup>

$$\Delta \simeq K^{1/2} D^{1/5} \Delta_0^{4/5}. \quad (72)$$

Finite charge stiffness  $K$  provides  $\mathcal{O}(\eta)$  corrections,

$$\eta = K^{-1/2}, \quad (73)$$

to the scaling laws in Eq. (72). To estimate them we note that at the first loop RG, one averages the non-linear term  $\mathcal{L}_{\text{bs}}$  over the *independent* Gaussian fluctuations described by the diagonal Gaussian action  $\mathcal{L}_0$ . Due to the factorization (45), the result of such an averaging can be represented in the form of the *product* of the contributions of the two independent Gaussian theories, with the terms of the action (46) scaling as

$$\frac{K}{l_{\text{ch}}^2} + \frac{1}{l_{\text{fl}}^2} + g_0 \left( \frac{l_{\text{fl}}}{a} \right)^{-\gamma_0} \left( \frac{l_{\text{ch}}}{a} \right)^{-\eta/4}. \quad (74)$$

Minimizing the composite-soliton action of the form (74) over *both*  $l_{\text{ch}}$  and  $l_{\text{fl}}$  amounts to including the coupling between the flavor and charge fluctuations by the non-linear term. The variational estimate yields

$$\frac{l_{\text{fl}}}{a} \simeq K^\alpha \left( \frac{D}{\Delta_0} \right)^{\frac{4}{5-\eta}}, \quad l_{\text{ch}} \simeq K^{\frac{1}{2}} l_{\text{fl}}, \quad \alpha = \frac{\eta}{10-2\eta} \quad (75)$$

for the correlation lengths, and produces the renormalized gap  $\Delta \simeq \hbar v K / l_{\text{ch}}$  that scales as

$$\Delta \simeq K^{\frac{1}{2}-\alpha} D^{\frac{1-\eta}{5-\eta}} \Delta_0^{\frac{4}{5-\eta}}. \quad (76)$$

The latter expression smoothly crosses over to the non-interacting case  $K = 1$ ,  $\Delta = \Delta_0$ , as well as has a correct scaling (72) in the classical limit  $K \rightarrow \infty$ .<sup>43</sup>

## VII. WEAK COUPLING LIMIT

### A. Integer density

The phase soliton treatment in the integer- $m$  case is simple in a sense that it is enough to keep the first term in the expansion (60). The saddle point (63) maps the problem onto that with  $U \equiv 0$  and

$$g_0 \rightarrow g_m = g_0 f_1^* J_m(2\tilde{A}) . \quad (77)$$

Using the results of the previous Section we obtain the renormalized minigaps

$$\Delta_m \simeq K^{1/2-\alpha} D^{\frac{1-\eta}{5-\eta}} \left( \Delta_m^{(0)}(\tilde{A}) \right)^{\frac{4}{5-\eta}} \quad (78)$$

[cf. Eq. (76)], and the bare minigaps

$$\Delta_m^{(0)}(\tilde{A}) = \Delta_0 |J_m(2\tilde{A})| \quad (79)$$

given by their noninteracting values (27) with the screened potential amplitude  $\tilde{A}$  defined in Eq. (39).

As noted in Ref. 24, the qualitative features of the noninteracting minigaps (27) persist in the interacting case. Namely, as a function of the *screened* potential amplitude (39), the minigaps (78) oscillate, vanishing at particular values of  $\tilde{A}$ . However, minigaps (78) are strongly *enhanced* in magnitude compared to (27) due to electron interactions. Also the dependence of the minigaps on both the bare backscattering  $\Delta_0$  and on the periodic potential amplitude  $A$  has a characteristic power law behavior which, in the limit of strong interactions  $K \gg 1$ ,

is given by a universal power law 4/5. This power law is a manifestation of the SU(4) flavor symmetry in the nanotube near half filling.

What is the cost of adding electron's *flavor* on top of its charge? As the problem is formally equivalent to that in the absence of the external potential, the results of Ref. 13 apply: On the energy scale below that of the frozen charge sector, the flavor sector is governed by the effective Gross-Neveu Lagrangian<sup>13,44</sup>

$$\begin{aligned} \mathcal{L}_{\text{GN}} &= \frac{\hbar v}{\pi} \int dx \left\{ \frac{1}{2} (\partial_\mu \theta^a)^2 - g_{\text{GN}} \sum_{a>b} \cos 2\theta^a \cos 2\theta^b \right\} \\ &= \hbar v \int dx \{ i \bar{\chi}_j \gamma_\mu \partial_\mu \chi_j - g_{\text{GN}} (\bar{\chi}_j \chi_j) (\bar{\chi}_{j'} \chi_{j'}) \} , \end{aligned} \quad (80)$$

where  $\chi_j$  are the Majorana fermions and the Gross-Neveu coupling in our case is  $g_{\text{GN}} \propto g_m$ . The excitations of the model (80) are *massive* relativistic particles transforming according to different representations of the O(6) group.<sup>45</sup> This analysis tells that the excitation gaps (27) that accidentally close in the noninteracting limit, do not close due to the effects of the fermionic exchange.

### B. Fractional density $m = 1/2$

Using the phase soliton method outlined in Sec. VIC above, we derive the effective phase mode Lagrangian

$$\mathcal{L}_{1/2}[\bar{\theta}^0, \bar{\theta}^a] = \mathcal{L}_0[\bar{\theta}^0, \bar{\theta}^a] + \mathcal{L}_{1/2}^{\text{int}}[\bar{\theta}^0, \bar{\theta}^a] \quad (81)$$

given by the sum of the Gaussian part  $\mathcal{L}_0$  [Eq. (47)] and the potential energy [see Appendix B for details]

$$-\mathcal{L}_{1/2}^{\text{int}} = \frac{\hbar v g_0'}{4\pi} \int dx \left\{ (4 - \kappa) v_{1/2}(2\tilde{A}) \mathcal{F}(2\bar{\theta}^0, 2\bar{\theta}^a) - \kappa v_{1/2}(2\tilde{A}) \sum_a \cos 2\bar{\theta}^0 \cos 2\bar{\theta}^a + \kappa u_{1/2}(2\tilde{A}) \sum_{a>b} \cos 2\bar{\theta}^a \cos 2\bar{\theta}^b \right\} . \quad (82)$$

Here the function  $\mathcal{F}$  is defined in Eq. (45) and the other quantities are defined in Appendix B.

Let us discuss the potential energy (82). Its first term has scaling dimension 3 and is irrelevant. The second term of the potential (82) is responsible for the charge excitation gap  $\Delta_{\text{ch}}$ . This term has scaling dimension

$$\gamma_{1/2} = 1 \quad (83)$$

and grows under the renormalization group flow. Finally, the third term is marginal. It describes the SU(4) *flavor* physics on the energy scale  $\Delta_{\text{fl}} \sim K^{-1/2} \Delta_{\text{ch}}$ .

Now we proceed to finding the gap for the charged excitation by considering the saddle-point optimization of the second term of the potential (82) by the neutral sector in a way similar to that described in Sec. VIA above. Adding an extra electron to the system (81) cor-

responds to a composite phase soliton in which the  $\bar{\theta}^a$  fields “switch” by  $\pi/2$  in the middle of a slow charged phase soliton, at the point when  $\cos 2\bar{\theta}^0 = 0$ . [It is possible to show<sup>41</sup> that although at this very point the effective sine-Gordon coupling  $\propto \cos 2\bar{\theta}^0$  for the neutral sector vanishes, the flavor soliton has a finite size and energy. This is the case since away from the center of the charged soliton,  $\cos 2\bar{\theta}^0 \neq 0$  giving the finite flavor scale.]

At the classical level, the neutral sector provides the bare potential  $\bar{\mathcal{F}}_{\text{cl}}^{(1/2)}$  from the saddle-point optimization

$$\sum_a \cos 2\bar{\theta}^0 \cos 2\bar{\theta}^a \rightarrow \bar{\mathcal{F}}_{\text{cl}}^{(1/2)}(\bar{\theta}^0) = - |\cos 2\bar{\theta}^0| . \quad (84)$$

By integrating over the quantum fluctuations of the flavor fields  $\bar{\theta}^a$  we obtain the flow of the form (68) with the scaling exponent (83) for the potential energy  $g_{1/2} \bar{\mathcal{F}}_{\text{cl}}^{(1/2)}(\bar{\theta}^0)$ ,

where

$$g_{1/2} = \frac{1}{4}\kappa g_0' |v_{1/2}(2\tilde{A})|. \quad (85)$$

From the self-consistency of the form (69) we find the flavor scale

$$l_{\text{fl},1/2} \sim \frac{a}{\kappa |v_{1/2}(2\tilde{A})|} \left( \frac{\epsilon_0}{\Delta_0} \right)^2, \quad (86)$$

[ $a$  is the tube radius], the renormalized coupling

$$g_{1/2}^* \simeq \frac{1}{l_{\text{fl},1/2}^2} \propto g_{1/2}^2, \quad (87)$$

and the scaling exponent

$$\tilde{\gamma}_{1/2} = 2 \quad (88)$$

for the classical optimized potential (84). As a result, the adjustment of the neutral sector yields the following effective potential for the charge mode:

$$V_{\text{charge}}^{(1/2)}[\bar{\theta}^0] = g_{1/2}^* \bar{\mathcal{F}}^{(1/2)}, \quad (89)$$

$$\bar{\mathcal{F}}^{(1/2)} = - \left| \bar{\mathcal{F}}_{\text{cl}}^{(1/2)} \right|^{\tilde{\gamma}_{1/2}} = -\frac{1}{2} \cos 4\bar{\theta}^0 + \text{const.}$$

Note that, due to the specific value of the scaling (83) [remarkably coinciding with the gap scaling for *noninteracting* fermions!], the renormalized potential  $\bar{\mathcal{F}}^{(1/2)}$  has only one Fourier harmonic, hence the coefficient 1/2 in Eq. (89) is not approximate [as one could anticipate from the analogous procedure leading to Eq. (58)], but *exact*. The functions  $\bar{\mathcal{F}}_{\text{cl}}^{(1/2)}$  and  $\bar{\mathcal{F}}^{(1/2)}$  are shown in Fig. 5. They both have a period  $\pi/2$  that corresponds to adding unit charge according to Eq. (42). The charge soliton in the present case has the *exact* form (59) with the correspondingly adjusted size  $l_{\text{ch}}$ .

The renormalized minigap  $\Delta_{1/2} \simeq K\hbar v/l_{\text{ch},1/2}$  can be found from the variational estimate of the form (74),

$$\frac{K}{l_{\text{ch},1/2}^2} + \frac{1}{l_{\text{fl},1/2}^2} + g_{1/2} \left( \frac{l_{\text{fl},1/2}}{a} \right)^{-1} \left( \frac{l_{\text{ch},1/2}}{a} \right)^{-\eta}, \quad (90)$$

yielding [ $\eta \equiv K^{-1/2}$ ]

$$\Delta_{1/2} \simeq K^{\frac{1-2\eta}{2-2\eta}} D \left[ \kappa |v_{1/2}(2\tilde{A})| \left( \frac{\Delta_0}{\epsilon_0} \right)^2 \right]^{\frac{1}{1-\eta}}. \quad (91)$$

The value of the gap (91) is strongly *enhanced* by the bandwidth  $D$  [even more so than for the integer- $m$  case of Sec. VII A] due to fluctuations of the flavor sector. We also note the  $m = 1/2$  incompressible state is explicitly interaction-induced. Indeed, although the charge excitation gap  $\Delta_{1/2}$  is derived in the strongly interacting limit  $K \gg 1$ , Eq. (91) gives a correct noninteracting limit  $\Delta_{1/2} = 0$  that is expected from the single particle Bloch theory. Formally, when  $K = 1$ , *both* flavor and charge

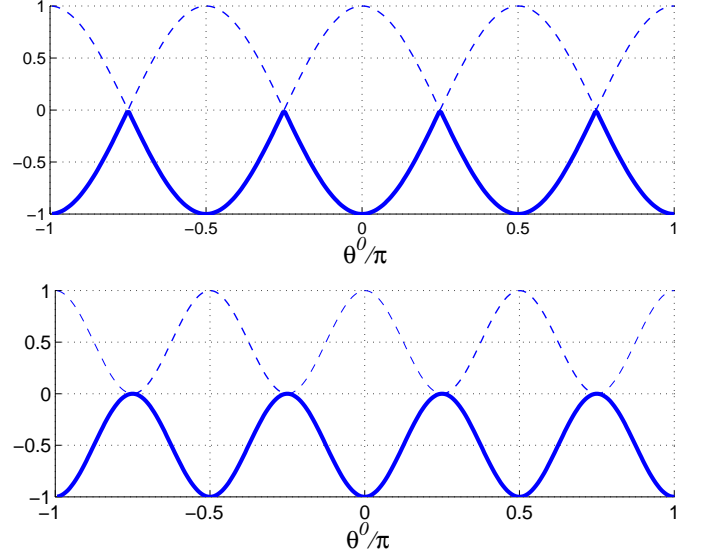


FIG. 5: Classical  $\bar{\mathcal{F}}_{\text{cl}}^{(1/2)}(\theta^0)$  (top) and renormalized  $\bar{\mathcal{F}}^{(1/2)}(\theta^0)$  (bottom) effective potentials (shown in bold) for the charge mode at density  $m = 1/2$  in the case of  $K \gg 1$ , Eqs. (89) and (84)

gaps are zero since the last two terms of the potential (82) vanish.

The weak coupling estimate (91) is valid when the flavor soliton size (86) is large,

$$l_{\text{fl},1/2} \gg \lambda_{\text{ext}}, \quad (92)$$

according to the condition (2) above. Practically, due to the large bandwidth  $D$ , Eq. (92) requires a very small bare gap  $\Delta_0$ . For typical values of parameters,  $\lambda_{\text{ext}} \sim 0.1 \mu\text{m}$  and  $\Delta_0 = 10 \text{meV}$ , the soliton scale defined in Eq. (86) is small compared to the potential period  $\lambda_{\text{ext}}$ ,  $l_{\text{fl},1/2} \sim 10 \text{nm} < \lambda_{\text{ext}}$ , and the condition (92) does not hold. In this case the excitation gap will be given by the strong coupling limit value  $\bar{\Delta}_{1/2}$  obtained below in Section VIII.

However, even for the above mentioned parameter values there are cases when the result (91) is applicable. This happens when the flavor soliton size  $l_{\text{fl},1/2}$  becomes large: either when one takes the tube that is almost metallic,  $\Delta_0 \sim 1 \text{meV}$ , in which case  $l_{\text{fl},1/2} \sim 1 \mu\text{m} > \lambda_{\text{ext}}$ , or for near certain potential amplitude values  $A^*$  that correspond to zeroes of the function  $v_{1/2}(2\tilde{A})$ , as shown in Fig. 8.

In the special case when the potential amplitude is such that the coupling  $g_{1/2}$  vanishes,  $v_{1/2}(2\tilde{A}) = 0$ , the charged excitation is *gapless* [similar to the integer  $m$  case considered above, where the gaps (78) vanish at the zeroes of the Bessel functions], but, as in the integer- $m$  case, *the flavor sector remains gapped*. Its gap  $\Delta_{\text{fl}}$  can be estimated from the effective  $\text{O}(6) \simeq \text{SU}(4)$  Gross-Neveu Lagrangian of the form (80) that is given by the last term of the Lagrangian (82), where now the coupling  $g_{\text{GN}} \propto u_{1/2}(2\tilde{A}^*) \neq 0$ . We stress that the resulting Gross-Neveu

coupling is a function of the external potential and thus, in principle, *can be externally controlled*.

## VIII. STRONG COUPLING LIMIT

### A. Lagrangian for the charged phase mode

Under the adiabaticity condition (65), the saddle point (64) combined with integrating over the fluctuations of the neutral sector [that has led to the renormalized Lagrangian (71)] yields the following Lagrangian for the charged mode:

$$\mathcal{L}_{\text{charge}}[\theta^0] = \frac{\hbar v}{\pi} \int dx \left( \frac{1}{2v^2} (\partial_t \theta^0)^2 - \frac{K}{2} (\partial_x \theta^0)^2 - g f_1^* \cos(4\theta^0 + m_{\text{tot}} k_{\text{ext}} x - 8\tilde{A} \sin k_{\text{ext}} x) \right), \quad (93)$$

where the density (1) is related to the chemical potential  $\mu$  by Eq. (40), where the coupling constant  $g$  is given by its renormalized value (54).

It is crucial to note that in the strong coupling limit (65), the renormalized coupling  $g \simeq 1/l_{\text{fl}}^2$  in the Lagrangian (93) does *not* depend on the density and on the external potential, as opposed to the weak coupling case of Section VII. Since this is a characteristic difference between the two limits that eventually yields to different excitation gap scaling, it is important to understand the physics behind it.

In the weak coupling limit the flavor soliton size  $l_{\text{fl}}$  depended on the external potential since the quantum fluctuations of the flavor sector were important on the scale of the potential period  $\lambda_{\text{ext}} < l_{\text{fl}}$ . Since the correlation length  $l_{\text{fl}}$  of the neutral sector was greater than the potential period, the flavor fluctuations were sensitive to the shape of the external potential. Naturally, in that case the parameters of the potential did influence the renormalization group flow.

In the present case,  $l_{\text{fl}} \ll \lambda_{\text{ext}}$ , and the renormalization group produces the effective coupling  $g$  [Eq. (54)] on the scale  $a < l < l_{\text{fl}}$  that appears “microscopic” for the external potential (10). In other words, the potential is adiabatic on the scale  $l < l_{\text{fl}}$ . However, a constant external potential has the same effect as the chemical potential. Although it can affect the local charge density, it does not affect the renormalization group flow. Thus both the flavor soliton scale  $l_{\text{fl}}$  and the renormalized coupling  $g$  in the strong coupling limit become independent

on the details of the external potential.

### B. Re-fermionization

The arguments that have led us to the charge mode Lagrangian (93) suggest an effective description of the strongly interacting nanotube electrons of four flavors in terms of a *single* mode. More precisely, we will assume below that one in fact can integrate out (eliminate) the neutral modes  $\theta^a$  from the system (46) completely under the following conditions: (i) as long as we are interested in the charging properties of the system on the energy scale  $\Delta_{\text{ch}} \gg \Delta_{\text{fl}}$  and on the spatial scale  $l \gg l_{\text{fl}}$  that are greater than those for the flavor sector; (ii) the flavor correlations (*i.e.* the effects of the fermionic exchange) are negligible.

The latter condition deserves a special attention. At very low energy scale (of the order of the exchange integral between the adjacent flavor soliton cores) the effects of the fermionic exchange can be important. However, in the limit (65) this energy scale can be made arbitrarily small. One can make a case<sup>27</sup> that the flavor correlations can be discarded when the temperature (assumed to be zero in this work) is very small but larger than this exchange scale, in which case the correct physical limit is to *trace over* all the possible flavor configurations.

To derive the effective single mode Hamiltonian for the nanotube in the strong coupling regime, we first present this Lagrangian in the canonical form suitable for subsequent re-fermionization by rescaling the charge mode:

$$\Theta = 2\theta^0 = \sum_{\alpha=1}^4 \Theta_{\alpha}. \quad (94)$$

The field  $\Theta$  is the displacement field for the total density,

$$\rho = \frac{1}{\pi} \partial_x \Theta. \quad (95)$$

To preserve correct commutation relations, the canonical momentum  $\Pi_{\Theta}$  for the field (94) should be half of that for the field  $\theta^0$ ,

$$\Pi_{\Theta} = \frac{1}{2} \Pi_{\theta^0} = \frac{1}{4} \sum_{\alpha=1}^4 \Pi_{\alpha}, \quad (96)$$

with  $\Pi_{\alpha}$  defined in Eq. (31). Changing variables in the Lagrangian (93) according to (94) and (96) we obtain the effective Lagrangian for the single mode  $\Theta$ ,

$$\mathcal{L}_{\text{eff}}[\Theta] = \frac{\hbar v'}{\pi} \int dx \left\{ \frac{1}{2v'^2} (\partial_t \Theta)^2 - \frac{K'}{2} (\partial_x \Theta)^2 - g \cos(2\Theta + m_{\text{tot}} k_{\text{ext}} x - 2\tilde{A}' \sin k_{\text{ext}} x) \right\}, \quad (97)$$

with the rescaled parameters

$$v' \equiv 4v, \quad K' \equiv \frac{K}{16}, \quad \text{and} \quad \tilde{A}' \equiv \frac{A}{K' \hbar k_{\text{ext}} v'} = 4\tilde{A}. \quad (98)$$

The re-definition of the parameters described by Eq. (98) has the following meaning. The velocity quadrupling simply states that we count incoming fermions regardless of their (four) flavors. The rescaling of the charge stiffness can be understood by noting that, with the same accuracy that has allowed us to discard the flavor modes, in the limit of  $K \gg 1$  one may write

$$K' \approx 1 + \frac{(K-1)}{16} \equiv 1 + \nu' V(q), \quad \nu' = \frac{1}{\pi \hbar v'}, \quad (99)$$

which is by definition the charge stiffness for the spinless Dirac fermions of velocity  $v'$  and density of states  $\nu'$  [cf. Eq. (36)]. Finally, the external fields  $U$  and  $\mu$  are not rescaled [cf. Eqs. (39) and (48)].

Re-fermionizing the Lagrangian (97) by introducing the Dirac spinors  $\Psi = (2\pi a')^{-1/2} e^{i\Theta}$ , we formally obtain the effective Hamiltonian

$$\mathcal{H}_{\text{eff}}[\Psi] = \int dx \Psi^\dagger \{ -i\hbar v' \sigma_3 \partial_x + \Delta' \sigma_1 + U(x) - \mu \} \Psi + \frac{1}{2} \sum_k \rho_k V(k) \rho_{-k} \quad (100)$$

for the fictitious spinless Dirac fermions. These are the NT electrons averaged (traced) over their SU(4) flavor configurations *with equal weights* (corresponding to temperature exceeding the exchange energy). Naturally, the total fermion number density (15) in the new variables

$$\rho(x) = \Psi^\dagger \Psi. \quad (101)$$

The effective gap  $\Delta'$  in Eq. (100) is chosen in such a way that it corresponds to the renormalized coupling (54) entering the Lagrangian (97),

$$g \simeq \frac{\Delta'}{\hbar v' a'}, \quad a' \simeq l_{\text{fl}} \quad (102)$$

similarly to the definition (35). In Eq. (102) the new length scale cutoff  $a'$  is assumed since the present approach is valid only at the length scales  $l > l_{\text{fl}}$  beyond the correlation length of the neutral sector.<sup>46</sup> Eq. (102) together with Eqs. (54) and (69) yields

$$\Delta' \simeq \frac{\hbar v'}{l_{\text{fl}}} \simeq D^{1/5} \Delta_0^{4/5}. \quad (103)$$

To summarize, we have shown that in the limit when the fermionic exchange is unimportant due to exponentially small overlap of the flavor solitons, the NT electron dynamics can be described by the effective Hamiltonian (100) of *spinless* Dirac electrons. These fictitious fermions of the density (15) interact with each other by the *same* Coulomb potential (16) as do the original nanotube electrons. We stress here that neither the Coulomb potential  $V(q)$  nor the external fields (external potential  $U(x)$  and the chemical potential  $\mu$ ) are renormalized, consistent with the fermions  $\Psi$  possessing the same electron charge as the original nanotube electrons.

### C. Excitation gaps

The (charge) excitation gaps can be now estimated from the effective Lagrangian (97) or from the Hamiltonian

(100). Below we consider the case

$$l_{\text{ch}} > \lambda_{\text{ext}} \quad (104)$$

of the charged excitation extended over several potential minima. In this case one can apply the standard phase soliton approach for the single mode.<sup>33</sup>

In the simplest case of integer *total* density  $m_{\text{tot}}$  one averages the potential term in the Lagrangian (97) over the potential period obtaining the effective coupling

$$g^{\text{strong}} = g J_{m_{\text{tot}}}(2\tilde{A}'), \quad (105)$$

performs integration over the quantum fluctuations of the  $\Theta$ -field

$$g^{\text{strong}}(l) = g^{\text{strong}}(a') \left( \frac{l}{a'} \right)^{-\eta'}, \quad \eta' = \frac{1}{\sqrt{K'}} \simeq 4\eta, \quad (106)$$

with  $K'$  given by Eq. (99) and  $\eta$  by Eq. (73), finds the corresponding charge soliton scale self-consistently as

$$g^{\text{strong}}(l_{\text{ch}}) \simeq \frac{K'}{l_{\text{ch}}^2}, \quad (107)$$

and obtains the excitation gap

$$\Delta_m^{\text{strong}} \simeq \left| J_{m_{\text{tot}}}(2\tilde{A}') \right|^{\frac{1}{2-\eta'}} \Delta^{\text{strong}}, \quad m_{\text{tot}} = 0, \pm 1, \pm 2, \dots \quad (108)$$

Here the charge gap

$$\Delta^{\text{strong}} \simeq K^{\frac{1-\eta'}{2-\eta'}} \Delta' \quad (109)$$

with  $\Delta'$  given by Eq. (103), and  $J_{m_{\text{tot}}} \equiv J_{4m}$  is the Bessel function that depends on the *total* density (1).

When the total density  $m_{\text{tot}} = p'/q'$  is a simple fraction, the charge density in the commensurate configuration is in general  $q' \lambda_{\text{ext}}$ -periodic. To derive the effective Hamiltonian for the charged phase mode, one needs to perform the standard phase soliton procedure for a single mode described by the Hamiltonian (97). For that, one performs the expansion

$$\Theta(x) = \bar{\Theta} + \Theta^{(1)} + \dots, \quad \Theta^{(n)} = \mathcal{O}(g^n) \quad (110)$$

in the *renormalized* coupling (54), solves the corresponding Euler–Lagrange equations, and finds the effective potential for the “slow” phase mode  $\bar{\Theta}$ . The resulting charge mode potential energy will be  $\mathcal{O}(g^q)$ . The corresponding excitation gap can be estimated as energy of the phase soliton  $\bar{\Theta}(x)$  (with quantum fluctuations of the  $\bar{\Theta}$  field taken into account if necessary).

#### D. Classical limit

The classical limit of the Hamiltonian (100) is obtained by discarding the  $\mathcal{O}(\eta')$  quantum fluctuations, and coarse-graining beyond the length scale  $l_{\text{fl}}$ . This amounts to discarding the zero-point motion of fermions and treating them as classical point-like particles [on the scale  $l > l_{\text{fl}}$ ] that interact with each other via the Coulomb potential. The classical energy of this system

$$E_{\text{cl}} = \sum_{i=1..N_e} (\Delta' + U(x_i)) + \sum_{j=1..N_h} (\Delta' - U(y_j)) \\ + \sum_{\substack{i,j=1 \\ i>j}}^{N_e} \frac{e^2}{|x_i - x_j|} + \sum_{\substack{i,j=1 \\ i>j}}^{N_h} \frac{e^2}{|y_i - y_j|} - \sum_{\substack{i,j=1 \\ i>j}}^{N_e, N_h} \frac{e^2}{|x_i - y_j|}. \quad (111)$$

Here  $N_e$  and  $N_h$  are the total number of electrons (with positions  $x_i$ ) and holes (with positions  $y_j$ ) in correspondingly minima and maxima of the external potentials (cf. Section II and Fig. 1). One can further introduce the cut-off for the long range Coulomb interactions by introducing the screening length  $l_s$  in the case when  $l_s < L$ , where  $L$  is the tube length, as well as include screening by the underlying substrate with the dielectric constant  $\varepsilon$  by substituting  $e^2 \rightarrow 2e^2/(\varepsilon + 1)$ .

It is instructive to follow the connection between the classical limit (111) of the effective Hamiltonian (100) and the original charge mode Lagrangian (97). For that, let us represent the coordinates of the classical electrons in the state with the total density (1) by

$$x_j = x_j^{(0)} + \phi_j, \quad (112)$$

where  $\phi_j$  are the displacements from the ideal positions

$$x_j^{(0)} = \frac{j\lambda_{\text{ext}}}{m_{\text{tot}}} \quad (113)$$

in the absence of the external potential. [For simplicity, we are not considering the holes in the maxima of  $U(x)$ , which can be treated analogously.] In the continual limit  $\phi_j \equiv \phi(x_j) \approx \phi(x)$  the charge density is

$$\rho(x_j) \approx \frac{m_{\text{tot}} \partial_x \phi}{\lambda_{\text{ext}}}, \quad (114)$$

describing the change of  $\phi$  by  $\lambda_{\text{ext}}/m_{\text{tot}}$  when one extra particle is added. The third sum in Eq. (111) gives the interaction energy between the electrons. Substituting the coordinates (112) into this sum and expanding it

up to the second order in  $\phi_i - \phi_j \approx (x_i^{(0)} - x_j^{(0)}) \partial_x \phi$ , we obtain the gradient term for the displacement mode energy,

$$\frac{1}{2} \int dx \left( 2e^2 \ln \tilde{N} \right) \rho^2(x) \equiv \frac{\hbar v'}{\pi} \int dx \frac{\tilde{K}' (\partial_x \Theta)^2}{2}, \quad (115)$$

where

$$\Theta = \frac{\pi m_{\text{tot}}}{\lambda_{\text{ext}}} \phi(x) \quad (116)$$

is the net charge mode (94) defined in accord with the expression (95) for the total charge density, and the charge stiffness

$$\tilde{K}' = \frac{1}{\pi \hbar v'} \cdot 2e^2 \ln \tilde{N} \simeq K' - 1 \approx K'. \quad (117)$$

Here the stiffness  $K'$  is defined in Eq. (99), and the argument  $\tilde{N}$  of the Coulomb logarithm is found self-consistently as a number of electrons that belong to the soliton that describes the charge excitation. The expression (115) is the classical limit of the second term of the Lagrangian (97) with a meaning of the Coulomb interaction between the quasi-classical electrons. The non-linear term of the Lagrangian (97) gives the energy cost  $\Delta' \cos(m_{\text{tot}} k_{\text{ext}} \delta \phi(x)) = \Delta'$  of adding one extra particle above the gap,  $\delta \phi = \lambda_{\text{ext}}/m_{\text{tot}}$  according to Eq. (114). This term corresponds to the first term the classical energy (111). The interaction with the potential  $U(x)$  can be written in the usual form (19) and added to the argument of the cosine via the gauge transformation (43).

#### E. Discussion

The main result of this Section is the single-mode effective Hamiltonian (100) that has allowed us to map the problem of the interacting fermions with the four flavors onto that of a single flavor and to utilize the standard phase soliton approach for the single mode.

The meaning of the present treatment is the following. In the noninteracting case, fermions of the same flavor avoid each other due to the Pauli principle. The ground state wave function is then given by a product of the four Slater determinants, one for each flavor. However, when the repulsion between the fermions is strong, fermions of *all* the flavors avoid each other in a similar way, and the ground state wave function is a Slater determinant of a four-fold size. This is manifest in the  $m_{\text{tot}} = 4m$ -dependence of the excitation gaps (108).

The original SU(4) flavor symmetry of the problem becomes manifest at the level of renormalization, namely in the particular scaling law of 4/5 of the renormalized gap (103) ‘produced’ via the renormalization group flow of the flavor sector at the length scales  $a < l < l_{\text{fl}}$ .

Let us discuss the results (108) and (109) in more detail. In the classical limit the charge excitation gap (109)

for the stand-alone nanotube has the same form as that obtained in Sec. VIE above, Eq. (72):

$$\Delta^{\text{strong}} = \Delta \quad \text{when} \quad K \rightarrow \infty. \quad (118)$$

However, one notes that the power law exponents in the expressions (109) and (108) are *different* from those in Eqs. (76) and (78). This is not surprising since the theory (93) is different from the original model (46). Whereas in the latter the exchange is important, in the former the flavor sector is traced over under the conditions specified above in Sec. VIII B. A similar situation has been observed in the recent calculation<sup>27</sup> for the spin-1/2 case and qualitatively explained in Ref. 47. We underline that the external potential (10), by adding an extra length scale  $\lambda_{\text{ext}}$ , naturally distinguishes the regimes  $l_{\text{fl}} > \lambda_{\text{ext}}$  and  $l_{\text{fl}} < \lambda_{\text{ext}}$  in which the flavor physics is important and unimportant, correspondingly. Accordingly, the dependence on the *parameters of the potential* in these two regimes is crucially different, as one may see by comparing *e.g.* Eqs. (78) and (108) *even in the limit*  $K \rightarrow \infty$ .

Finally, we have shown that the energy (111) is a classical limit of the strong coupling Hamiltonian (100) and, therefore, the classical limit of the whole problem (46) of strongly interacting nanotube electrons in the external fields. It is not surprising that the strongly interacting regime of the problem is adiabatically connected to its classical limit; that is what is expected from the saddle-point approximation, with the quantum corrections around this saddle point yielding the renormalized Dirac gap  $\Delta'$ . What is remarkable is that, due to the Dirac nature of the nanotube spectrum and to the massive Thirring — sine-Gordon correspondence, the bosonization utilized in the present work is essentially exact and therefore allowed us to go all the way to the classical limit of the strongly interacting problem utilizing the saddle point treatment of the bosonic action of the four modes.

## IX. PHASE DIAGRAM

In the present Section we will utilize the effective Hamiltonian (100) and its classical limit (111) to draw the phase diagram in the  $A, \mu$  plane, Fig. 6, where  $A$  is the potential amplitude in Eq. (10). In this diagram, each region in Fig. 6 corresponds to a particular commensurate phase with the density of  $n_e = N_e/N$  electrons and  $n_h = N_h/N$  holes per potential period, with  $N = L/\lambda_{\text{ext}}$  [ $L$  is the tube length]. Such regions are labeled by pairs  $(n_e, n_h)$  as described in Section II, with the total density

$$m_{\text{tot}} = 4m = n_e - n_h \quad (119)$$

corresponding to Eq. (1). The underlying Dirac symmetry makes the phase diagram symmetric with respect to  $\mu \leftrightarrow -\mu$ ,  $n_e \leftrightarrow n_h$ , so that only the  $\mu > 0$  part is shown.

Below we will consider the classical limit (111) and will mainly focus on completely delocalized charged ex-

citations (at large screening radius),

$$l_{\text{ch}} \sim l_s > L. \quad (120)$$

The nanotube in this case can be viewed as a sequence of quantum dots and anti-dots that are induced by the minima and maxima of the external potential. These dots are equivalent and in this respect the system becomes translational invariant if one neglects effects of the finite system size  $L$ . Hence in the limit (120), by raising the chemical potential one adds an electron (hole) to *every* potential minimum (maximum), which results in adding  $\sim N = L/\lambda_{\text{ext}} \gg 1$  particles to the tube of the length  $L$ . As a consequence, first, *all* of the charge states characterized by the *total* density  $m_{\text{tot}}$  [ $m_{\text{tot}}$  either integer or fractional] are incompressible; second, excitation gaps as a function of the potential amplitude  $A$  *never vanish* due to the charging energy  $\sim \ln N$  of the Coulomb repulsion between the particles added into the different minima or maxima of  $U(x)$ .

The phase diagram can be obtained by minimizing the energy functional

$$E_{\text{cl}} - \mu(N_e - N_h) \quad (121)$$

with respect to positions  $x_i$  and  $y_i$  of electrons and holes in the following way. We neglect the finite system effects and utilize translational invariance. In this case the optimal positions of electrons and holes relative to each potential minimum (maximum) are the same. To find them we minimize the functional

$$E_{n_e, n_h}(A) - \mu(n_e - n_h) \quad (122)$$

[which is the functional Eq. (121) per potential period], where the corresponding potential energy values calculated per  $\lambda_{\text{ext}}$  are

$$E_{10} = \Delta' - A + \frac{e^2}{\lambda_{\text{ext}}} \sum_{n=1}^{N/2} \frac{1}{n}, \quad (123)$$

$$E_{11} = 2E_{10} - \frac{2e^2}{\lambda_{\text{ext}}} \sum_{n=1}^{N/2} \frac{1}{n - \frac{1}{2}}, \quad (124)$$

$$E_{20} = \min_{\delta x} \left\{ 2\Delta' - 2A \cos k_{\text{ext}} \delta x + \frac{e^2}{2\delta x} + \frac{e^2}{\lambda_{\text{ext}}} \sum_{n=1}^{N/2} \left( \frac{2}{n} + \frac{1}{n + \frac{2\delta x}{\lambda_{\text{ext}}}} + \frac{1}{n - \frac{2\delta x}{\lambda_{\text{ext}}}} \right) \right\} \quad (125)$$

and so forth. While minimizing the energy  $E_{n_e, n_h}$  with respect to the positions of electrons and holes within each potential period, unphysical configurations of electrons on top of the holes are excluded by demanding that their minimum separation be  $e^2/\Delta'$ . The latter condition takes into account the maximum exciton binding energy in the Dirac system.

Each border separating regions with different  $(n_e, n_h)$  is itself comprised of incompressible states with higher

fractions  $m$ , as shown by the domain  $(1/2, 0)$  between  $(0, 0)$  and  $(1, 0)$ , characteristic of the devil's staircase behavior<sup>29</sup>. The fractional total density  $m_{\text{tot}} = 1/2$  state  $(1/2, 0)$  has an electron in every other potential minimum (Fig. 1a).

Let us further simplify the functional  $E_{n_e, n_h}(A)$  by minimizing the interaction energy between the charges only in the *same* potential minimum (or maximum), treating the rest of the system in a mean-field way:

$$E_{n_e, n_h} \approx (n_e + n_h)(\Delta' - A) + \frac{(n_e - n_h)^2 e^2}{2C_0} + V_{n_e} + V_{n_h}. \quad (126)$$

The first term in (126) is an energy of  $n_e$  electrons placed into each minimum and  $n_h$  holes into each maximum of  $U(x)$ . It corresponds to the first two terms of (111). The second term in (126) is the interaction energy of positive and negative charges located in the extrema of  $U(x)$ . Here

$$C_0 = \frac{\lambda_{\text{ext}}}{2 \ln(L/\lambda_{\text{ext}})} \quad (127)$$

is a NT capacitance per period  $\lambda_{\text{ext}}$ . If the screening length is smaller than system size,  $l_s < L$ , then  $L$  should be substituted by  $l_s$  in Eq. (127). Finally,  $V_n$  in (126) is the interaction energy of  $n$  electrons (or  $n$  holes) minimized with respect to their positions inside the corresponding potential well of the periodic potential (10). The Dirac symmetry yields  $E_{n_e, n_h} = E_{n_h, n_e}$ .

Let us study the phase diagram in more detail. For simplicity, consider *integer*  $n_e$  and  $n_h$ . Due to the Dirac symmetry, it is enough to consider the case  $\mu > 0$  corresponding to  $n_e \geq n_h$ . Minimization of Eq. (121) using the approximation (126) yields the phase diagram

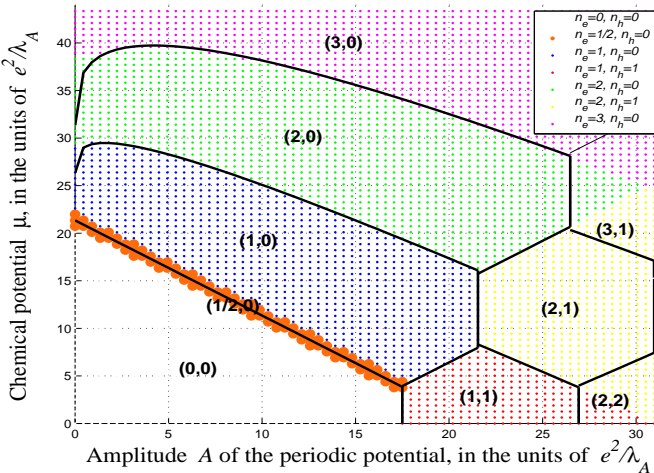


FIG. 6: Phase diagram for the nanotube,  $\Delta' = 6\pi e^2/\lambda_{\text{ext}}$ ,  $\ln(L/\lambda_{\text{ext}}) = 2.5$ ,  $e^2/\lambda_{\text{ext}} = 1.44$  meV for  $\lambda_{\text{ext}} = 1\mu\text{m}$ . Color regions are the result of numerical minimization, black lines are approximations obtained from Eq. (126) with  $V_n$  given by Eq. (132).

sketched in Fig. 7. Energy gaps corresponding to the incompressible states with the total density  $n = n_e - n_h = (n_e + 1) - (n_h + 1) = \dots = (n_e + s) - (n_h + s)$  oscillate but do not vanish. Their minimum value

$$\delta\mu_{n_e, n_h}^{\text{min}} = \frac{e^2}{C_0} \quad (128)$$

is determined by the NT charging energy. The regions  $(n_e, n_h)$  and  $(n_e + 1, n_h + 1)$  of the phase diagram are separated by the vertical lines of fixed  $A$ , with its value implicitly determined from

$$A = \Delta' + \frac{1}{2} (V_{n_e+1}(A) - V_{n_e}(A) + V_{n_h+1}(A) - V_{n_h}(A)). \quad (129)$$

Away from the values (129) the gap increases  $\propto A$ .

The model (126) can be treated exactly in the limiting cases of a few and of a large number of particles per each potential minimum. The former case relates to the phase diagram of Fig. 6 at  $e^2/\lambda_{\text{ext}} < A \lesssim \Delta'$ . The latter one is interesting since the corresponding excitation gaps cross over with those obtained in Section VIII [Eq. (108)]. In this case the phase diagram for the large  $A$  becomes universal (Fig. 7). Below we consider both cases.

#### A. Small density $n_e, n_h \sim 1$

The results of the numerical energy minimization (color in Fig. 6) can be fairly accurately reproduced (solid lines) by applying the approximation (126) for the case of a few particles per potential minimum (maximum). Below we will calculate the corresponding energies  $V_n$ , Eqs. (132).

When the Coulomb interaction over a period is small,

$$\frac{e^2}{\lambda_{\text{ext}}} \ll A \lesssim \Delta', \quad (130)$$

one can estimate the energies  $V_{n_e, n_h}(A)$  by approximating each potential well of (10) by a quadratic polynomial:

$$U(x) \approx -A + \min_{n \leq N} \frac{Ak_{\text{ext}}^2}{2} (x - (n + \frac{1}{2})\lambda_{\text{ext}})^2. \quad (131)$$

Minimizing the Coulomb energy of  $n$  charges in the potential (131), one obtains the values  $V_n$ :

$$\begin{aligned} V_0 &= V_1 = 0, \\ V_2 &= 3(\pi/2)^{2/3} \left(\frac{e^2}{\lambda_{\text{ext}}}\right)^{2/3} A^{1/3}, \dots \\ V_3 &= 5^{2/3} V_2(A), \dots \end{aligned} \quad (132)$$

The power law correction  $\sim A^{1/3}$  due to the above expressions is observed in Fig. 6 for  $A \sim \Delta'$  as a deviation from the straight lines that separate different regions of the phase diagram.

For the yet smaller values of the potential amplitude  $A \ll e^2/\lambda_{\text{ext}}$ , the above perturbative treatment of interaction breaks down (solid lines in Fig. 6 deviate from the borders between the phase diagram regions obtained from the numerics). In this case it can be shown that the perturbation theory in  $A$  yields a regular behavior of the gap widths in accord with the numerics in Fig. 6.

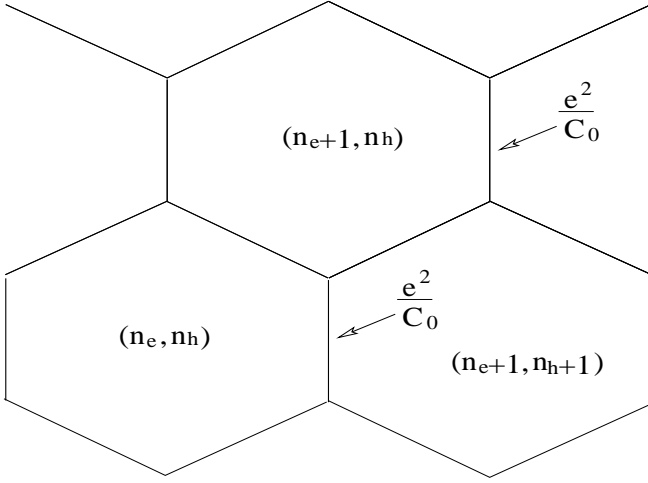


FIG. 7: Phase diagram in the  $(A, \mu)$  plane according to the model (126). The minimum width of the gap for the incompressible state with any density  $n_e - n_h$  is given by the NT charging energy (128). In the limit  $n_e, n_h \gg 1$  all the regions of the phase diagram are identical, with their period in  $A$  given by Eq. (137).

### B. Large density $n_e, n_h \gg 1$

At large  $n_e, n_h \gg 1$  the model (126) can be simplified by using the continuous description for the density of the classical electrons (holes) inside each potential minimum (maximum). In this case, utilizing the Thomas–Fermi approximation, the charge density  $\rho(x)$  in each minimum can be represented by the continuous function

$$\rho(x) \approx \rho_{\text{TF}} = -\frac{\pi n_e}{\lambda_{\text{ext}}} \cos k_{\text{ext}} x \quad (133)$$

that mimics the external potential profile (10). The density (133) is normalized to  $n_e = \int_{\lambda_{\text{ext}}/4}^{3\lambda_{\text{ext}}/4} \rho_{\text{TF}}(x) dx$ . The interaction energy  $V_{n_e}$  or  $V_{n_h}$  inside each “quantum dot” can be estimated as

$$V_{n_e} \simeq \frac{e^2}{2} \int_{\lambda_{\text{ext}}/4}^{3\lambda_{\text{ext}}/4} dx dx' \frac{\rho_{\text{TF}}(x) \rho_{\text{TF}}(x')}{|x - x'|} \equiv \frac{n_e^2 e^2}{2C_1}, \quad (134)$$

where the “dot capacitance”

$$C_1 = \frac{\lambda_{\text{ext}}}{2\pi \ln \frac{\lambda_{\text{ext}}}{a'}} \quad (135)$$

is independent of the potential amplitude  $A$ . The singularity in the integral in Eq. (134) is cut off on the scale  $a' \sim l_{\text{fl}}$  of the order of the flavor soliton size, below which the quasichlassical description breaks down. The  $A$ -dependence of  $C_1$  would appear as a correction to  $V_{n_e}$  with  $A$ -dependent integration limits in Eq. (134). The case  $V_{n_h}$  of the holes in the potential maxima (“anti-dots”) is analogous. Eq. (129) then yields the potential amplitude values that separate the configurations

$(n_e, n_h)$  and  $(n_e + 1, n_h + 1)$ :

$$A_{(n_e, n_h) \rightarrow (n_e+1, n_h+1)} = \Delta' + \frac{e^2}{2C_1} (n_e + n_h + 1). \quad (136)$$

In this limit all the “honeycomb” regions of the phase diagram in Fig. 7 are identical with their period in  $A$  being

$$\delta A_{n_e, n_h} = \frac{e^2}{C_1}. \quad (137)$$

Qualitatively, the honeycomb structure of Fig. 7 appears already for the moderate amplitudes  $A$ , as it can be seen in Fig. 6. The borders between the regions of the phase diagram in the limit  $A > e^2/\lambda_{\text{ext}}, \Delta'$ , are approximately linear, dominated by the linear dependence of  $E_{n_e, n_h}$  on  $A$  that stems from the first term of Eq. (126).

### C. Crossover with the quantum case

Let us now show that the asymptotic values of the positions (136) of the gap minima derived in the previous subsection coincide with those derived in Section VIII utilizing the phase soliton approach, assuming a finite screening length  $l_{\text{ch}} \sim l_s \sim \lambda_{\text{ext}}$ .

Consider the positions of the minima for excitation gaps (108) (as a function of the potential amplitude)

$$\tilde{A}' = 4\tilde{A} = \frac{4A}{K\epsilon_0} \approx \frac{\pi}{2} \cdot \frac{A}{e^2/C_1}, \quad (138)$$

where we took the value of the charge stiffness (36) at the momentum scale  $\lambda_{\text{ext}}^{-1}$  and substituted  $K \rightarrow K - 1$  at  $K \gg 1$ . Utilizing the asymptotic behavior of the  $s$ -th zero of the Bessel function  $J_n$ ,

$$2\tilde{A}'_n^{(s)} \simeq \text{const} + \frac{\pi n}{2} + \pi s \quad (139)$$

[cf. Eqs. (108), (78), and (27)], we obtain the values of  $A \simeq (n_e + n_h)e^2/2C_1$  in accord with Eq. (136). Here we made the obvious identifications  $n \equiv m_{\text{tot}} = n_e - n_h$  and  $s = \min\{n_e, n_h\}$ . Away from these critical values the gap increases linearly in  $A$  similarly to what was stated above [after Eqs. (129) and (137)].

## X. QUANTIZED CURRENT

Below we discuss the experimental means of detecting and measuring the minigaps. A conventional way to detect excitations is to measure the differential finite-bias conductance as a function of gate voltage and potential amplitude. This procedure could allow one to directly map the phase diagram of the system.

A more exciting, although less trivial way is to realize for the first time the Thouless pump<sup>28</sup> in a nanotube.

Such a setup requires adiabatically moving periodic potential that could be created *e.g.* by coupling to a surface acoustic wave,<sup>24</sup> or by sequentially modulated gate voltages on the array of underlying gates. When the chemical potential is inside the  $m$ -th minigap  $\Delta_m$ , the adiabatically moving periodic potential with frequency  $f$  will induce *quantized current*<sup>24</sup>

$$j = m_{\text{tot}} e f, \quad m_{\text{tot}} = 4m, \quad m = \pm 1, \pm 2, \dots \quad (140)$$

in the nanotube.

In such a setting, novel fractional- $m$  incompressible states considered in this work will manifest themselves in the adiabatic current (140) quantized in the corresponding *fractions* of  $4ef$ . This result can be understood by revoking the topological invariant property of the Thouless current.<sup>28</sup> The current (140) is trivial in a semiclassical limit, having a meaning of transporting on average  $m_{\text{tot}}$  electrons per cycle in a conveyor-belt fashion. By staying inside the gap and adiabatically changing the parameters of the system, Eq. (140) remains invariant and hence valid in the fully quantum-mechanical case.

Operation of the charge pump requires adiabaticity

$$k_B T, \quad h f \ll \Delta_m, \quad (141)$$

where  $\Delta_m$  is a (renormalized) minigap, and  $T$  is temperature. Since the energy scale for the minigaps is set either by the gap at half-filling, or by the strength of the Coulomb interactions between electrons separated by  $\sim \lambda_{\text{ext}}$ , the typical minigap values  $\Delta_m$  will be in the meV range, and the adiabaticity condition (141) is realistic. Furthermore, a similar SAW setup applied to pumping electrons between the two 2D electron gases through a pinched point contact<sup>48</sup> has almost metrological accuracy;<sup>49,50</sup> recently the SAW-assisted adiabatic pumping through the laterally defined quantum dot has also been demonstrated.<sup>51</sup>

We contrast the non-dissipative current (140) *on the plateau* with the dissipative non-quantized current away from commensuration considered in Ref. 52 for arbitrary quantum wire. Such a *non-quantized* current is pumped when no gap opens (for incommensurate densities or for commensurate densities with the interaction below criticality) and is characterized by the interaction-dependent critical exponents.<sup>52</sup>

A practical realization of the proposed pumping setup could become a first implementation of the Thouless transport. Besides being instrumental in studying electron interactions in a nanotube (by detecting and measuring fractional minigaps that arise solely due to interactions), it could realize the “conveyor belt” for electrons with a possibility of pumping current quantized in fractions of the unit charge. In other words, such a setup would make the first example of the charge pump operating at the *fraction of the base frequency*, pumping on average a fractional number of electrons per period. This setup would allow one to study in detail the electron correlations and interactions in nanotubes, with having a

variety of controllable experimental parameters at hand, such as the shape and frequency of the external potential, nanotube Dirac gap  $\Delta_0$  (that can be modified by a parallel magnetic field), and the gate voltage. By exploring the phase diagram one can study effects of Wigner crystallization, quantum commensurate-incommensurate transitions, and the Tomonaga-Luttinger correlations.

Finally we note that the described setup can be utilized to adiabatically transport the low-energy strongly correlated SU(4) *flavor* states (*e.g.* those obeying the effective Gross-Neveu Lagrangian (80) described in Sec. VII) over a macroscopic distance, since the coupling to the adiabatically moving external potential is SU(4) invariant and thus it does not destroy spin or flavor correlations. Such a system could become useful in the context of solid state implementations of quantum computers, as well as for realizing a quantized spin-polarized pump by subjecting the system to magnetic field.

## XI. CONCLUSIONS

We have shown that coupling of the interacting nanotube electrons to an external periodic potential is a very rich setup that allows one to study a number of effects of strongly correlated 1d fermions. The Dirac nature of the nanotube spectrum near half-filling allowed us to treat the problem of massive strongly interacting fermions non-perturbatively, and to develop the phase soliton method for the four interacting fermion modes.

In particular, we demonstrated how increasing the electron-electron interactions and the curvature of the electronic dispersion (controlled by the Dirac gap) drives the system from the Luttinger liquid of four modes into the Wigner crystal. While in the former limit the excitation gaps arise due to the Bragg diffraction of the delocalized quasiparticles of the four flavors, the latter limit maps onto the problem of the semi-classical commensurate-incommensurate transitions. Formally, this mapping has been achieved through the saddle-point treatment of the bosonized sine-Gordon action of the four modes. The saddle point in the limit of strong interactions has yielded the effective spinless Dirac Hamiltonian for the nanotube in the Wigner crystal regime.

We also discussed the adiabatic charge pump setup to study the phase diagram experimentally. In this setup one could detect the interaction-induced incompressible electron states, study electron-electron interactions and transition to the Wigner crystal regime in greater detail, as well as realize the quantized charge pump (“Archimedean screw”) that pumps a fraction of electron charge per cycle due to electron interactions.

## Acknowledgments

It is a pleasure to thank Leonid Levitov for bringing this problem to the author’s attention and for fruitful discus-

sions. This work was initiated at MIT (supported by NSF MRSEC grant DMR 98-08941) and completed at Princeton (supported by NSF MRSEC grant DMR 02-13706).

### APPENDIX A: CONDITIONS FOR THE TIGHT-BINDING LIMIT

Below we derive the condition (29) for the tight binding limit (28) in the single particle picture. We consider the two cases depending on the relation between the potential amplitude  $A$  and the Dirac mass term  $\Delta_0$ .

The case  $A \ll \Delta_0$  corresponds to the “nonrelativistic limit” of the Dirac equation, where all the relevant energies are much smaller than the gap  $\Delta_0$ . We define the “Dirac” electron mass  $M$  as

$$\Delta_0 = Mv^2. \quad (\text{A1})$$

This allows for the Schrödinger description, in full analogy with the non-relativistic limit of the Dirac equation in quantum electrodynamics. The corresponding Hamiltonian

$$\mathcal{H}_{\text{Sch}} = -\frac{\hbar^2}{2M} \partial_x^2 + U(x). \quad (\text{A2})$$

Tunneling amplitude between the adjacent minima of  $U(x)$  is proportional to  $e^{-S|_{A < \Delta_0}/\hbar}$ , where the classical action under the barrier

$$S|_{A < \Delta_0} = \frac{4\hbar\sqrt{A\Delta_0}}{\epsilon_0}. \quad (\text{A3})$$

Therefore both the minibands and tunneling are suppressed in the limit  $A \ll \Delta_0$  if

$$\left(\frac{\Delta_0}{\epsilon_0}\right)^{-1} < \frac{A}{\epsilon_0} \ll \frac{\Delta_0}{\epsilon_0}. \quad (\text{A4})$$

The inherently Dirac regime occurs when  $A > \Delta_0$ . In this case electron can tunnel between the minima of the potential (10) sequentially through the hole part of the spectrum. The corresponding tunneling amplitude  $\sim e^{-2S|_{A > \Delta_0}/\hbar}$ , where the classical action under barrier between the electron and hole parts is

$$S|_{A > \Delta_0} = \frac{1}{v} \int dx \sqrt{|(E - U(x))^2 - \Delta_0^2|}. \quad (\text{A5})$$

Tunneling from the minimum of  $U(x)$  at  $E = \Delta_0 - A$  to the hole part of the spectrum yields ( $\zeta \equiv \Delta_0/A$ )

$$\begin{aligned} S|_{A > \Delta_0} &= \frac{2\hbar A}{\epsilon_0} \left\{ \sqrt{\zeta} - (1 - \zeta) \ln \frac{1 + \sqrt{\zeta}}{\sqrt{1 - \zeta}} \right\} \\ &= \frac{4\hbar\Delta_0^{3/2}}{\epsilon_0 A^{1/2}} \left( \frac{1}{1 \cdot 3} + \frac{\zeta}{3 \cdot 5} + \frac{\zeta^2}{5 \cdot 7} + \dots \right). \end{aligned} \quad (\text{A6})$$

Tunneling from the energy level  $|E| \ll 2A$  far from the potential bottom yields the action  $S \simeq \pi\Delta_0^2/\hbar v\mathcal{E}$ , where

$\mathcal{E} = |\partial_x U(x)|$ . As a result we obtain that the single particle bandwidth in the Dirac regime is exponentially suppressed if

$$\frac{\Delta_0}{\epsilon_0} < \frac{A}{\epsilon_0} < \left(\frac{\Delta_0}{\epsilon_0}\right)^c, \quad (\text{A7})$$

where the exponent  $c = 3$  for tunneling from the potential minimum and  $c = 2$  for tunneling from energy level far from the potential bottom.

Summarizing, Eqs. (A4) and (A7) yield the condition (29) for the tight-binding limit (28).

### APPENDIX B: $m = \frac{1}{2}$ PHASE SOLITON ACTION

Below we consider the weak coupling limit for the fractional density  $m = 1/2$  characterized by the chemical potential  $\tilde{\mu} = \frac{1}{4}$  in accord with Eq. (40).

Our course of action has been outlined in Section VI above. Technically, it will be more convenient to first work in the basis of the original fields  $\Theta_\alpha$  and later utilize the transformation (41) to obtain the Lagrangian  $\mathcal{L}_{1/2}[\tilde{\theta}^0, \tilde{\theta}^a]$  in the charge-flavor basis. Since the average of the potential energy (48) over the *two* successive potential periods is zero, we decompose the fields  $\Theta_\alpha(x)$  in a series in the coupling  $g_0$  keeping the first two orders

$$\Theta_\alpha = \bar{\Theta}_\alpha + \Theta_\alpha^{(1)}, \quad \Theta_\alpha^{(1)} = \mathcal{O}(g_0). \quad (\text{B1})$$

The Euler – Lagrange equations for the Hamiltonian (38) yield

$$\Theta_\alpha^{(1)}{}_{xx} + \frac{K-1}{4} S_{xx}^{(1)} = -\frac{g_0}{2} \sin\left(2\bar{\Theta}_\alpha + \frac{1}{2}k_{\text{ext}}x - 2\tilde{A} \sin k_{\text{ext}}x\right), \quad (\text{B2})$$

where  $S = \sum \Theta_\alpha$ . Integrating Eq. (B2) we obtain

$$\Theta_\alpha^{(1)}{}_x = \frac{1-K}{4} S_x^{(1)} + \frac{g_0}{k_{\text{ext}}} \tilde{\Theta}_\alpha, \quad (\text{B3})$$

$$S_x^{(1)} = \frac{g_0}{Kk_{\text{ext}}} \sum \tilde{\Theta}_\alpha, \quad (\text{B4})$$

$$\tilde{\Theta}_\alpha = \sum_m \frac{J_m(2\tilde{A})}{1-2m} \cos\left(2\bar{\Theta}_\alpha + \left(\frac{1}{2} - m\right)k_{\text{ext}}x\right) \quad (\text{B5})$$

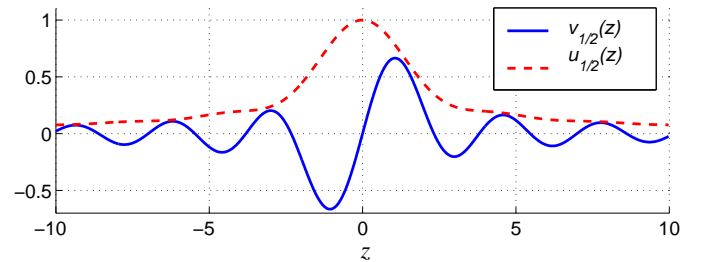


FIG. 8: The functions  $v_{1/2}$  and  $u_{1/2}$  defined in Eqs. (B9) and (B10). We find that  $v_{1/2}(z) < u_{1/2}(z)$  holds for all  $z$ . Zeros of  $v_{1/2}$ :  $z = 0, \pm 2.33, \pm 3.80, \pm 5.47, \dots$

Substituting Eqs. (B3) and (B5) into the Hamiltonian (38), after somewhat lengthy but straightforward algebra

the slow mode potential follows:

$$V_{1/2} = \frac{\hbar v g'_0}{16\pi} \int dx \left\{ (4 - \kappa) v_{1/2}(2\tilde{A}) \sum_{\alpha} \cos 4\bar{\Theta}_{\alpha} + \kappa \sum_{\alpha \neq \alpha'} \left( u_{1/2}(2\tilde{A}) \cos(2\bar{\Theta}_{\alpha} - 2\bar{\Theta}_{\alpha'}) - v_{1/2}(2\tilde{A}) \cos(2\bar{\Theta}_{\alpha} + 2\bar{\Theta}_{\alpha'}) \right) \right\} \quad (\text{B6})$$

Here

$$g'_0 = \left( \frac{g_0}{k_{\text{ext}}} \right)^2 = \left( \frac{\Delta_0}{\epsilon_0 a} \right)^2, \quad (\text{B7})$$

$$\kappa = \frac{K - 1}{K}, \quad (\text{B8})$$

and the functions  $v_{1/2}$  and  $u_{1/2}$  are defined as

$$v_{1/2}(z) = \sum_{m=-\infty}^{\infty} \frac{J_m(z) J_{1-m}(z)}{(2m-1)^2}, \quad (\text{B9})$$

$$u_{1/2}(z) = \sum_{m=-\infty}^{\infty} \left( \frac{J_m(z)}{1-2m} \right)^2 \quad (\text{B10})$$

with  $z$  being a shorthand for  $2\tilde{A}$ . The functions  $v_{1/2}(z)$  and  $u_{1/2}(z)$  are plotted in Fig. 8.

In the commensurate state we find that the minimum value

$$\min V_{1/2}[\bar{\Theta}_{\alpha}] = -\frac{\hbar v g'_0}{4\pi} \int dx \left\{ 4|v_{1/2}(2\tilde{A})| + \kappa u_{1/2}(2\tilde{A}) \right\} \quad (\text{B11})$$

of the potential (B6) corresponds to the slow modes  $\{\bar{\Theta}_{\alpha}\}$  being an arbitrary permutation of a set  $\{\phi_1 \phi_1 \phi_2 \phi_2\}$ , with  $\phi_{1,2} = \pm\pi/4$  for  $v_{1/2}(2\tilde{A}) > 0$  and  $\phi_1 = 0, \phi_2 = \pi/2$  for  $v_{1/2}(2\tilde{A}) < 0$ .

Let us now discuss the symmetry of the obtained commensurate classical state. The ground state degeneracy in the noninteracting case ( $\kappa = 0$ ) is equal to  $2^4$ . This follows from the potential (B6) in which only the first term is nonzero. We find that in the presence of interactions ( $\kappa > 0$ ), the other terms in (B6) reduce this degeneracy from 16 to six. This result could have been foreseen without any calculation since the remaining degeneracy is just a number of configurations in which any two *different* fields,  $\Theta_{\alpha}$  and  $\Theta_{\beta}$  with  $\alpha \neq \beta$ , are placed in the same minimum of the external potential. In other words, in the bosonized treatment the effect of fermionic *exchange* manifests itself in a stronger repulsion between the solitons of the same flavor. This is in agreement with the numerical minimization performed in Sec. VI B, Fig. 4. The symmetry of the obtained classical ground state is schematically illustrated in Fig. 1(e).

The change of variables (41) in the potential (B6) yields Eq. (82).

\* Electronic address: [dima@alum.mit.edu](mailto:dima@alum.mit.edu)

<sup>1</sup> S. Iijima, *Nature* **354**, 56-58 (1991)

<sup>2</sup> R. Saito, G. Dresselhaus and M. S. Dresselhaus, *Physical Properties of Carbon Nanotubes*, Imperial College Press, London, 1998.

<sup>3</sup> M.S. Dresselhaus, G. Dresselhaus, Ph. Avouris, *Carbon Nanotubes: Synthesis, Structure, Properties and Applications*, Springer Verlag, New York, 2001

<sup>4</sup> P.L. McEuen, *Nature* **393**, 15 (1998)

<sup>5</sup> C. Dekker, *Physics Today*, May 1999, p. 22

<sup>6</sup> P.M. Ajayan and O.Z. Zhou, in the book<sup>3</sup>

<sup>7</sup> P. Avouris, *Acc. Chem. Res.* **35**, 1026 (2002)

<sup>8</sup> D. Rotman, *Technology Review* **105**, 37 (March 2002)

<sup>9</sup> Y.A. Krotov, D.-H. Lee, S.G. Louie, *Phys. Rev. Lett.* **78**, 4245 (1997)

<sup>10</sup> R. Egger, A. O. Gogolin, *Phys. Rev. Lett.* **79**, 5082 (1997)

<sup>11</sup> C. Kane, L. Balents, M. P. A. Fisher, *Phys. Rev. Lett.* **79**, 5086 (1997)

<sup>12</sup> A. Odintsov and H. Yoshioka, *Phys. Rev. Lett.* **82**, 374 (1999)

<sup>13</sup> L. S. Levitov, A. M. Tsvelik, *Phys. Rev. Lett.* **90**, 016401 (2003); [cond-mat/0205344](https://arxiv.org/abs/cond-mat/0205344)

<sup>14</sup> M. Stone (Ed.), *Bosonization*, World Scientific, Singapore (1994)

<sup>15</sup> M. Bockrath, D. H. Cobden, P. L. McEuen, N. G. Chopra, A. Zettl, A. Thess, R. E. Smalley, *Science* **275**, 1922 (1997)

<sup>16</sup> S. Tans, M.H. Devoret, R. Groeneveld and C. Dekker, *Nature* **394** 761 (1998)

<sup>17</sup> M. Bockrath, D. H. Cobden, Jia Lu, A. G. Rinzler, R. E. Smalley, L. Balents, P. L. McEuen, *Nature* **397**, 598 (1999)

<sup>18</sup> Z. Yao, H. W. Ch. Postma, L. Balents, C. Dekker, *Nature* **402**, 273 (1999)

<sup>19</sup> J. Nygard, D.H. Cobden, M. Bockrath, P.L. McEuen, P.E. Lindelof, *Applied Physics A* **69**, 297 (1999)

<sup>20</sup> H. Ishii, H. Kataura, H. Shiozawa, H. Yoshioka, H. Otsubo, Y. Takayama, T. Miyahara, S. Suzuki, Y. Achiba, M. Nakatake, T. Narimura, M. Higashiguchi, K. Shimada, H. Namatame and M. Taniguchi, *Nature (London)* **426**, 540 (2003)

<sup>21</sup> D.S. Novikov, preprint [cond-mat/0412456](https://arxiv.org/abs/cond-mat/0412456)

- <sup>22</sup> S. Coleman, Phys. Rev. D **11**, 2088 (1975)
- <sup>23</sup> F.D.M. Haldane, J. Phys. A **15**, 507 (1982)
- <sup>24</sup> V.I. Talyanskii, D.S. Novikov, B.D. Simons, L.S. Levitov, Phys. Rev. Lett. **87**, 276802 (2001); [cond-mat/0105220](#)
- <sup>25</sup> C.L. Kane, Ranjan Mukhopadhyay, and T.C. Lubensky, Phys. Rev. Lett. **88**, 036401 (2002)
- <sup>26</sup> M. Ogata and H. Shiba, Phys. Rev. B **41**, 2326 (1990)
- <sup>27</sup> V.V. Cheianov and M.B. Zvonarev, Phys. Rev. Lett. **92**, 176401 (2004); J. Phys. A **37**, 2261 (2004)
- <sup>28</sup> D. J. Thouless, Phys. Rev. B **27**, 6083 (1983)
- <sup>29</sup> P. Bak, Rep. Prog. Phys. **45**, 587 (1982)
- <sup>30</sup> J. Frenkel and T.A. Kontorova, Zh. Eksp. Teor. Fiz. **8**, 1340 (1938)
- <sup>31</sup> F.C. Frank and J.H. van der Merwe, Proc. Roy. Soc. **198**, 205, 216 (1949)
- <sup>32</sup> I.E. Dzyaloshinsky, Zh.E.T.F. **47**, 1420 (1964);
- <sup>33</sup> V.L. Pokrovsky, A.L. Talapov, Sov. Phys. JETP **75**, 1151 (1978);
- <sup>34</sup> D. P. DiVincenzo and E. J. Mele, Phys. Rev. B **29**, 1685 (1984)
- <sup>35</sup> C. L. Kane and E. J. Mele, Phys. Rev. Lett. **78**, 1932 (1997)
- <sup>36</sup> C. Zhou, J. Kong, and H. Dai, Phys. Rev. Lett. **84**, 5604 (2000); M. Ouyang, J.L. Huang, C.L. Cheung, C.M. Lieber, Science **292**, 5517 (2001)
- <sup>37</sup> H. Ajiki and T. Ando, J. Phys. Soc. Jpn. **65**, 505 (1996).
- <sup>38</sup> J. -O. Lee, J. R. Kim, J. J. Kim, J. Kim, N. Kim, J. W. Park, and K. H. Yoo, Sol. Stat. Comm. **115**, 467 (2000).
- <sup>39</sup> To be precise, this statement is true in the forward scattering approximation that holds down to undetectably small energies where interaction-induced gaps may open.<sup>9–12</sup>
- <sup>40</sup> The author thanks A.M. Polyakov for a discussion on renormalization
- <sup>41</sup> D.S. Novikov, unpublished
- <sup>42</sup> K. Wilson, Phys. Rev. **179**, 1499 (1969); C.G. Callan, Phys. Rev. D **2**, 1541 (1970); K. Symanzik, Commun. Math. Phys. **18**, 227 (1970)
- <sup>43</sup> Similar expression for renormalized gap  $\Delta$  has been obtained earlier in Ref. 13. Whereas we agree on scaling exponents of  $D$  and  $\Delta_0$ , the  $K$ -dependence is different. The procedure of Ref. 13 yields the prefactor  $K^{1/5}$  instead of the more natural result  $K^{1/2+\mathcal{O}(\eta)}$  that matches the classical limit. We believe this discrepancy is a consequence of oversimplifying the renormalization group treatment by introducing a *single* soliton scale under the RG in Ref. 13.
- <sup>44</sup> D.J. Gross and A. Neveu, Phys. Rev. D **10**, 3235 (1974)
- <sup>45</sup> A.B. Zamolodchikov and Al.B. Zamolodchikov, Ann. Phys. **120**, 253 (1979)
- <sup>46</sup> Here we also do not distinguish between  $\ln(l_s/a)$  and  $\ln(l_s/a')$  in the Coulomb formfactor  $V(q)$ , with large  $K \gg 1$  implying large screening length  $l_s \sim l_{ch} \gg a, a'$ . This corresponds to treating the tube *capacitance* with logarithmic accuracy.
- <sup>47</sup> G.A. Fiete and L. Balents, Phys. Rev. Lett. **93**, 226401 (2004)
- <sup>48</sup> J.M. Shilton, V.I. Talyanskii, M. Pepper, D.A. Ritchie, J.E.F. Frost, C.J.B. Ford, C.G. Smith, G.A.C. Jones, J. Phys. Condens. Matter **8**, L531 (1996); V.I. Talyanskii, J.M. Shilton, M. Pepper, C.G. Smith, C.J.B. Ford, E.H. Linfield, D.A. Ritchie, G.A.C. Jones, Phys. Rev. B **56**, 15180 (1997).
- <sup>49</sup> Q. Niu, Phys. Rev. Lett. **64**, 1812 (1990)
- <sup>50</sup> J. Cunningham, V.I. Talyanskii, J.M. Shilton, M. Pepper, A. Kristensen, P.E. Lindelof, J. Low Temp. Phys. **118**, 555 (2000)
- <sup>51</sup> J. Ebbecke, N.E. Fletcher, T.J.B.M. Janssen, F.J. Ahlers, M. Pepper, H.E. Beere, and D.A. Ritchie, Appl. Phys. Lett. **84**, 4319 (2004); preprint [cond-mat/0312304](#)
- <sup>52</sup> R. Citro, N. Andrei, and Q. Niu, Phys. Rev. B **68**, 165312 (2003)